

AD718902

Reproduced by
**NATIONAL TECHNICAL
INFORMATION SERVICE**
Springfield, Va. 22151

D D C
RECEIVED
FEB 23 1971
B.

40

**BEST
AVAILABLE COPY**

AD 718 902

Semi-Annual Technical Report No. 1
(for period June 22, 1970 to Dec. 31, 1970)

Title: Structure and Property Control through
Rapid Quenching of Liquid Metals

Contract No. : DAHC15 70 C 0283
ARPA Order No.: 1608
Program Code No.: OD10

Name of Contractor:
Massachusetts Institute of Technology
Cambridge, Massachusetts 02139

Principal Investigator:
N. J. Grant
(617) 864-6900 Ext. 5638

Effective date of Contract: June 22, 1970
Contract Expiration Date: June 21, 1971

Total Amount of Contract: \$233,000.

Sponsored by:
Advanced Research Projects Agency
ARPA Order No. 1608

DISTRIBUTION STATEMENT A
Approved for public release;
Distribution Unlimited

D D C
RECEIVED
FEB 23 1971
RECEIVED
B

DOCUMENT CONTROL DATA - R&D

(Security classification of title, body of abstract and indexing annotation must be entered when the overall report is classified)

1. ORIGINATING ACTIVITY (Corporate author) Massachusetts Institute of Technology Cambridge, Mass 02139		2a. REPORT SECURITY CLASSIFICATION unclassified	
		2b. GROUP	
3. REPORT TITLE Structure and Property Control Through Rapid Quenching of Liquid Metals			
4. DESCRIPTIVE NOTES (Type of report and inclusive dates) Semi-annual Technical Report #1, (July 1, 1970- Dec. 31, 1970)			
5. AUTHOR(S) (Last name, first name, initial) Grant, Nicholas J.; Pelloux, Regis M.N.; Flemings, Merton C; Argor, All S.			
6. REPORT DATE Jan. 1, 1971		7a. TOTAL NO. OF PAGES 77	7b. NO. OF REFS
8a. CONTRACT OR GRANT NO. DAHC15 70 C 0283 A. PROJECT NO. ARPA Order #1608 c. Program Code #OD10 d.		9a. ORIGINATOR'S REPORT NUMBER(S)	
		9b. OTHER REPORT NO(S) (Any other numbers that may be assigned this report)	
10. AVAILABILITY/LIMITATION NOTICES			
11. SUPPLEMENTARY NOTES		12. SPONSORING MILITARY ACTIVITY Advanced Research Projects Agency 1400 Wilson Blvd. Arlington, Va. 22209	
13. ABSTRACT The first results of the processing of coarse metal powders of maraging 300 and IN 100 are reported. The effect of cooling rates on the dendrite structure of maraging 300 alloy has been investigated in a wide range of cooling rates. The structure of atomized particles are presented and their cooling rates are derived from the dendrite arm spacings. The size and distribution of inclusions in a commercial 300 grade maraging has been determined and related to the mechanical properties (tensile and fatigue). The analysis of the stress and strain conditions around an inclusion as a function of the overall state of stress is being investigated in order to determine the crack initiation criteria.			

DD FORM 1473
1 JAN 68

unclassified

Security Classification

14. KEY WORDS	LINK A		LINK B		LINK C	
	ROLE	WT	ROLE	WT	ROLE	WT
Rapid Quenching Structure Control Segregation Control						

INSTRUCTIONS

1. **ORIGINATING ACTIVITY:** Enter the name and address of the contractor, subcontractor, grantee, Department of Defense activity or other organization (corporate author) issuing the report.
- 2a. **REPORT SECURITY CLASSIFICATION:** Enter the overall security classification of the report. Indicate whether "Restricted Data" is included. Marking is to be in accordance with appropriate security regulations.
- 2b. **GROUP:** Automatic downgrading is specified in DoD Directive 5200.10 and Armed Forces Industrial Manual. Enter the group number. Also, when applicable, show that optional markings have been used for Group 3 and Group 4 as authorized.
3. **REPORT TITLE:** Enter the complete report title in all capital letters. Titles in all cases should be unclassified. If a meaningful title cannot be selected without classification, show title classification in all capitals in parentheses immediately following the title.
4. **DESCRIPTIVE NOTES:** If appropriate, enter the type of report, e.g., interim, progress, summary, annual, or final. Give the inclusive dates when a specific reporting period is covered.
5. **AUTHOR(S):** Enter the name(s) of author(s) as shown on or in the report. Enter last name, first name, middle initial. If military, show rank and branch of service. The name of the principal author is an absolute minimum requirement.
6. **REPORT DATE:** Enter the date of the report as day, month, year, or month, year. If more than one date appears on the report, use date of publication.
- 7a. **TOTAL NUMBER OF PAGES:** The total page count should follow normal pagination procedures, i.e., enter the number of pages containing information.
- 7b. **NUMBER OF REFERENCES:** Enter the total number of references cited in the report.
- 8a. **CONTRACT OR GRANT NUMBER:** If appropriate, enter the applicable number of the contract or grant under which the report was written.
- 8b, c, & 8d. **PROJECT NUMBER:** Enter the appropriate military department identification, such as project number, subject number, system numbers, task number, etc.
- 9a. **ORIGINATOR'S REPORT NUMBER(S):** Enter the official report number by which the document will be identified and controlled by the originating activity. This number must be unique to this report.
- 9b. **OTHER REPORT NUMBER(S):** If the report has been assigned any other report numbers (either by the originator or by the sponsor), also enter this number(s).
10. **AVAILABILITY/LIMITATION NOTICES:** Enter any limitations on further dissemination of the report, other than those

imposed by security classification, using standard statements such as:

- (1) "Qualified requesters may obtain copies of this report from DDC."
- (2) "Foreign announcement and dissemination of this report by DDC is not authorized."
- (3) "U. S. Government agencies may obtain copies of this report directly from DDC. Other qualified DDC users shall request through _____."
- (4) "U. S. military agencies may obtain copies of this report directly from DDC. Other qualified users shall request through _____."
- (5) "All distribution of this report is controlled. Qualified DDC users shall request through _____."

If the report has been furnished to the Office of Technical Services, Department of Commerce, for sale to the public, indicate this fact and enter the price, if known.

11. **SUPPLEMENTARY NOTE:** Use for additional explanatory notes.

12. **SPONSORING MILITARY ACTIVITY:** Enter the name of the departmental project office or laboratory sponsoring (paying for) the research and development. Include address.

13. **ABSTRACT:** Enter an abstract giving a brief and factual summary of the document indicative of the report, even though it may also appear elsewhere in the body of the technical report. If additional space is required, a continuation sheet shall be attached.

It is highly desirable that the abstract of classified reports be unclassified. Each paragraph of the abstract shall end with an indication of the military security classification of the information in the paragraph, represented as (TS), (S), (C), or (U).

There is no limitation on the length of the abstract. However, the suggested length is from 150 to 225 words.

14. **KEY WORDS:** Key words are technically meaningful terms or short phrases that characterize a report and may be used as index entries for cataloging the report. Key words must be selected so that no security classification is required. Identifiers, such as equipment model designation, trade name, military project code name, geographic location, may be used as key words but will be followed by an indication of technical context. The assignment of links, rules, and weights is optional.

TABLE OF CONTENTS

TASK I	PROCESSING OF ALLOYS	
	I. Introduction	
	II. Experimental Work	
	A. Melting & Atomization	1
	B. Powder Characterization	3
	C. High Treatment Response	5
	D. Cleaning	6
	E. Chemistry	7
	F. Powder Consolidation	8
TASK II	SOLIDIFICATION RESEARCH	
	-Abstract-	1
	-Introduction	2
	I Effect of Cooling Rate on Structure of Maraging 300 Alloy	2
	-Levitation Melting & Casting-	3
	-Unidirectional Casting-	4
	-Vacuum Melting & Furnace Cooling-	5
	II Analysis of Structure & Heat Flow of Atomized Particles	5
	-Structure of Atomized Particles-	6
	-Heat Flow During Atomization-	7
	III Rapid Solidification of Metal Alloys	10
	-Conclusion-	12
TASK III	THERMOMECHANICAL TREATMENTS	
	I Heat Treatment and Aging of 300 Grade Maraging Steel	1
	-Metallography-	2
	-Tensile Properties-	3
	-Fatigue-	5
TASK IV	MICROSTRUCTURE AND MECHANICAL PROPERTIES	
	Introduction	1
	I Plastic Strain and Triaxial Stress Fields in the Neck of Circumferentially Grooved Tensile Specimens	1
	II Tensile Deformation of Vascomax 300	3
	III Plane-Strain Fracture Toughness and Stress Corrosion Cracking Experiments	4

Task I

PROCESSING OF ALLOYS

IMT

1. Introduction

The general technical philosophy of advancing the state of art of modern complex alloys through a powder metallurgy approach has been fully described in the proposal entitled "Structure and Property Control Through Rapid Quenching of Liquid Metals". In brief summary, powder metallurgy promises to produce alloys of much greater chemical and structural homogeneity and refinement than is possible by the historic "ingot-hot work" route. These chemical and structural improvements will result in improved levels of hot workability, uniformity and strength of alloys to which powder technology can be successfully applied. The powder approach also promises to provide a process tool for development of alloys hitherto limited in alloy content by severe ingot segregation with its unfavorable effects on hot workability.

The present work will be concerned with "prealloyed" powders produced by atomization of fully alloyed liquid metal. If liquid metal is generally classed as a liquid, a description of every practical way developed to date for atomization of liquids may be found in Orr¹. These methods include pressure nozzles, including jet injection, fan, swirl, and impact nozzles; two-fluid atomizers in which the liquid stream is disintegrated by a high-velocity stream of gas; impinging-type nozzles wherein two liquid streams collide; vibrating nozzles using sonic or mechanical energy; and rotating cups or dishes in which droplets are generated at the outer rim. The patent literature indicates that many of these processes have been used for liquid metals. However, the physical and chemical constraints of handling liquid metals without contamination have resulted in only a few practical processes for production of highly alloyed powders. Among several current commercial processes which may be noted are: (1) Federal-Mogul which is a two-fluid process employing high purity argon for liquid metal stream disintegration, (2) Whittaker "Rotating Electrode Process" (a version of the rotating disc) in which the end of a rotating bar is arc melted in a high purity inert atmosphere and fine droplets flung off by centripetal force, and (3) Homogeneous Metals in which a "pressure nozzle", operating between the pressure difference of a hydrogen filled chamber in which the liquid metal stands and a "vacuum"

¹ C. Orr, Jr. "Particulate Technology", Mac millan Co., N. Y. 1966, p. 19-34.

chamber, generates a fine droplet spray. These processes produce "state of the art" powders but are generally expensive to operate and the fine powders require careful handling. The Whittaker process, for example, requires a generation of a centerless ground alloy ingot bar for the feedstock before powder making even begins. The remaining two processes produce fine powders (-20 mesh, Homogeneous Metals, and -60 mesh, Federal Mogul). Atomization mechanics for these processes require liquid metal nozzles of 1/4" (6 mm) diameter or less with consequent low throughput rates. Some correlation "laws" relating particle size to atomization parameters have been given by Lubanska¹ for "two-fluid" atomization systems of liquid metals.

Powder making art must be considered growing and capable of further significant development. For the present program it was considered germane to use a fully developed steam atomization process for production of coarser powders. This process is cheap to operate, has large capacity by virtue of metal stream diameters in the range 9 to 12 mm, and permits approximately a one decade range of median particle size through adjustment of atomization parameters. Coarse powder has also been found easy to handle without contamination.

Two alloys were selected for the program, the first a "state of the art" nickel base alloy with fully documented physical and mechanical properties, and the second a maraging steel which presents problems potentially solved by powder metallurgy. The relevance of these alloys and the applicability of the powder approach is discussed below.

High strength nickel base alloys are widely used as components of modern gas turbine power systems. For example, nickel and cobalt base alloys combined make up 50% of the weight of advanced jet aircraft engines. Most high temperature nickel base alloys in use today consist of a nickel-chromium matrix strengthened by gamma prime precipitate, $Ni_3(Al, Ti)$, with further additions of solid solution strengtheners such as cobalt, molybdenum, tungsten, tantalum and columbium as well as a carbide system. The metallurgy of these alloys has been reviewed by Decker.²

¹ H. Lubanska, Journal of Metals, February 1970, p. 45.

² R. F. Decker, "Strengthening Mechanisms in Nickel-Base Superalloys". Market Development Department, International Nickel Company.

With the most advanced alloys of this group, the fabricability and reproducibility of the mechanical properties have continuously represented grave problems. Several "state of the art" alloys can only be used in the "as cast" condition because of their lack of formability at any temperature. The designer is consequently forced to design to the low side of a wide scatter band.

For the program, the alloy IN-100 was selected as a first experimental material. It is a "cast only" alloy with the highest volume percent of gamma prime of existing commercial alloys. It is exceedingly difficult to fabricate. The powder approach is expected to make a major contribution in processing by permitting fabrication of this alloy by hot work. Engineering properties are fully described in a bulletin, "Engineering Properties of IN-100 Alloy".¹

The powder approach has already been applied to IN-100.² Extrusion, vacuum hot pressing, pancake forging, and hot isostatic pressing have been used for densification.

The product is characterized by fine grain size, structural uniformity and superplastic behavior under certain hot work conditions. However, the high temperature creep properties have not been evaluated and the basic factors governing grain size control are incompletely investigated. These areas, as well as effects of hot isostatic pressing conditions on structure, will be more fully probed in the current program.

The second alloy chosen for this program was an 18% Ni maraging steel. A particular commercial alloy, Vascomax 300, was selected. Maraging steels are characterized by very high strength and excellent formability.³

Alloy composition is basically low carbon, $\leq .03\%$, 18% nickel, 9% cobalt, 5% molybdenum, 0.6% titanium and 0.1% aluminum. In the solution annealed condition, the structure is essentially martensite plus a small percentage of retained austenite. The low ($.03\%$ max.) carbon martensite is soft and tough and can be machined and formed. Solution annealing or austenitizing is carried out at 1500°F .

¹ International Nickel Company.

² S. H. Richman, B. W. Castledine, and J. W. Smythe, "Superalloy P/M Components for Elevated Temperature Applications", S.A.E. Congress, Detroit, Michigan, January, 1970.

³ Product Bulletin "18% Nickel Ultra High Strength Maraging Steels", Vasco, Latrobe, Pa.

Upon cooling, transformation to martensite starts at $M_s = 310^\circ\text{F}$. Finish of transformation is at $M_f = 210^\circ\text{F}$ with percentage completion depending on chemical homogeneity and structure. Since 210°F is above room temperature, the normal martensite structure following anneal is explained. Aging or maraging occurs at 900°F by precipitation of Ni_3Mo ribbons on dislocations in the martensite and a Ni-Ti or Fe-Ti phase.¹ Reversion of martensite to austenite does not occur significantly at the aging temperature of 900°F . For the Vascomax 300 alloy, UTS of 294,000 and 0.2% Y.S. of 290,000 is specified.

Metallurgically, the maraging steels have certain problems. When the molten alloy cools in ingot form, the last metal to solidify is rich in nickel, molybdenum and titanium. This segregation can persist throughout reduction to final mill form. It is decreased but is not eliminated by increased working and homogenization at 2300°F .² Its occurrence in the final microstructure is denoted as "banding".

Since these steels are used in high stress applications, the effects of banding on transverse properties can be significant. Fracture toughness also becomes a critical design criterion. One characteristic of these steels possibly originating in chemical and structural inhomogeneity is a wide scatter band of fracture toughness for given yield strength levels.³ The presence of titanium carbides at prior austenite grain boundaries may also decrease toughness.⁴

¹ A.M. Hall, C. J. Slunder; "The Metallurgy Behavior and Application of 18-Percent Nickel Maraging Steels", NASA SP-5051, 1968, p. 28-33.

² Ibid. NASA SP-5051, p. 38-41.

³ A. A. Coleman, "High Strength Maraging Steels for Tactical Missile Rocket Motors", Rocketdyne Division of North American Aviation Report No. R-4384, July 1966, p 8-7.

⁴ Boniszewski, T.; and Boniszewski, Elspeth: "Inclusions in 18 Ni-Co-Mo Maraging Steel", J. Iron & Steel Institute, Vol. 204, 4 April '66, pp 360-365.

To date no literature on prealloyed powder metallurgy of maraging steel has been uncovered. The possible benefits of a powder approach to maraging steels thus include the following:

1. elimination of banding,
2. decrease in scatter of fracture toughness,
3. increase in transverse properties,
4. increased fracture toughness,
5. the possibility of alloy design with greater amounts of Ni_3Mo strengthening.

Higher molybdenum alloys have been tentatively explored.¹ Practically they would appear to be limited by severe segregation if the ingot route is followed. The powder approach could very well permit a new generation of maraging steels.

¹Mihalisin, J. R.; and Bieber, C. G.: Progress Toward Attaining Theoretical Strength with Iron-Nickel Maraging Steels. *Journal of Metals*, Vol. 18, No. 9, September '66, pp 1033-1036.

II. Experimental Work

A. Melting and Atomization

Melting and atomization were carried out in equipment which was designed to produce coarse powder in the size range 500 to 5000 microns. The equipment was capable of being set up for steam, argon or nitrogen atomization. Essential features included the following:

1. 30 lb. Ajax induction furnace with automatic power factor control,
2. MgO crucibles,
3. Argon inert gas cover maintained at ≈ 15 cfh during purging and melting,
4. Leeds and Northrup recording Pt - Pt 10% Rh thermocouples (disposable) for liquid metal temperature measurement,
5. Conical tundish lined with B & W Kaocrete 32, covered and preheated to $\gt 1800^{\circ}\text{F}$,
6. Zirconia tundish nozzles; diameters 10, 11.9 and 12.7 mm depending on atomization requirements,
7. Steam atomization with top and side nozzles,
8. Argon and nitrogen atomization with side nozzle only,
9. Steam or gas pressures measured at the nozzles,
10. Water quench tank for collecting coarse powder.

Melt dip samples were taken for every melt just before tap as soon as the metal bath had been heated to its predetermined tap temperature. Titanium and aluminum melt additions were made ≈ 1 minute before tap.

The above arrangement was used for Heat Nos. 136 to 171 inclusive as detailed in Table I. Analysis of powders from these heats, which were all maraging steel except 149, indicated that oxygen pick up and titanium and aluminum loss after the metal left the furnace were major problems. Accordingly, the atomization arrangement was improved to eliminate oxide entrainment and pick-up during tap from the furnace to the tundish. The new arrangement featured the following improvements which have been used from Ht. No. 172 to date:

1. Raised atomization cabinet 30". This effectively decreased free fall

- height from furnace to tundish pool from $\approx 24"$ to $\approx 5"$.
2. Installation of a "tight" fitting castable Fiberfrax tundish cover.
 3. Use of an argon purge @ 30 cfh in tundish during tap with tundish cover in place.
 4. Use of $\approx .015"$ Ni melt out plugs in tundish to permit slag rise before atomization.
 5. Use of an $MgO - Al_2O_3$ tundish wash (Lamag 31) to decrease contact of liquid metal with SiO_2 phases in Kocrete 32 tundish refractory.
 6. Complete stripping of tundish of all previous skull and rewash with Lamag 31 before each heat.

The results of these improvements are still subject to current chemical analysis. Observation has indicated complete elimination of spatter in the tundish and effective functioning of the melt out plug to hold up tundish flow for $\approx 1-2$ seconds before atomization. This new arrangement also permits lower tap temperatures since the "in place" tundish cover cuts down radiation cooling of the top of the tundish liquid metal pool.

One critical experiment was carried out during atomization of Ht. No. 173, see Table I. In this case the argon atomization was interrupted and a chill mold sample of the metal stream from the tundish nozzle taken 1" below the nozzle at the point of atomization. Analysis of this sample for oxygen, titanium and aluminum, which is currently in progress, will permit a more exact definition of the oxygen pick-up mechanics in the present atomization system.

A summary of all melting and atomization runs carried out to date is given in Table I. The median particle size and standard deviation is also given here for each heat. Adjustment of tundish nozzle diameter was primarily used to achieve a median particle size of ≈ 2000 microns. Decreasing tap temperatures, argon atomization and titanium and aluminum additions as well as improved tundish practice were all used to improve chemistry control of the powders.

While powder characteristics are discussed in the next section, a few comments can be made about melting experience with the two alloys in this program. Both VM-300 and IN-100 contain titanium and aluminum. These elements have such low partial pressures of oxygen at equilibrium at $2600 - 2900^\circ F$ that slag formation inevitably occurs. The slags are thin in both cases and very adherent and stringy in the case of IN-100 under argon cover. During argon, nitrogen or steam atomization the tundish

stream of maraging steel VM-300 breaks up fully at the atomization point. IN-100, on the other hand, was closely observed during argon atomization, Ht. No. 175. The metal stream was deformed into a wide, thin sheet indicating that with this alloy in an oxidizing atmosphere, surface tension does not act to form droplets from the edges of a thin liquid sheet. A flake-like powder (see next section) results.

B. Powder Characterization

Coarse powders produced by steam, argon and nitrogen atomization were characterized by shape, screen analysis, packing density, and oxide inclusions. Samples were forwarded to MIT for dendrite spacing measurement and further microscopic study.

IN-100 atomized by either steam or argon (Ht. Nos. 149 and 175, respectively, Table I) results in sharp twisted flakes with a thin adherent coat of oxide, Figure 1. There was a substantial fraction of + 3 1/2 mesh in both cases. Size analysis was not carried out. The shapes of these powders are unfavorable for processing since they present many reentrant cavities and folds in cleaning, and have a very low packing density in hot isostatic pressing or extrusion cans. Nevertheless, the usefulness of coarse powder atomization in reducing the dimensional scale of segregation is clearly illustrated by comparing Figures 2 and 3. Figure 2 is the dendrite structure of - 3 1/2/+4 mesh flake (0.5 mm long x 1/2 mm thick), Ht. No. 149. Figure 3 is the dendrite structure of 3" cast bar used as a typical remelt stock. In the cast bar, both primary δ and primary carbides occur as large separate segregated phases. In the coarse powder, the scale of this segregation is reduced by a full order of magnitude. This reduction in the scale of segregation is expected to greatly increase the hot workability of powder compacts of this alloy.

For the IN-100 alloy, a backup "fine" powder produced by vacuum atomization has been acquired to permit continuation of work on compaction, hot work and property determination. Details of the evaluation of this powder will be reported later.

Maraging steel Vascomax 300 coarse powder produced by steam, argon and nitrogen atomization was, with only two exceptions, substantially spherical in all cases and coated with a black oxide shell which had spalled off on some particles. The exceptions to the generally spherical particle shapes were the coarser fractions (+8) of heats 170 and 171 where titanium and aluminum additions were made to the melts. The behavior tended toward that of IN-100 in terms of flake-like shape because of the presence of these two elements.

Figure 4 shows an "as atomized" and cleaned sample of the full particle size range of Ht. No. 148. The cleaning process, as described later, produces a bright shiny powder well suited for hot isostatic pressure or extrusion.

Size analysis using a U. S. Standard Sieve Series was run on the total powder of each maraging steel heat with the exception of 166 and 167. Results are presented in log probability - log size form (see Figure 13 for a typical figure). Median particle sizes and standard deviations are listed for each heat in Table I, the median particle size (50% size) indicated in each figure.

While atomization parameters were not explored over wide ranges, several comparisons can be made indicating effects operating in coarse powder production. Ht. Nos. 169 and 176 were atomized under substantially the same conditions except (Table I) for tundish nozzle (metal stream) diameter. The 12.7 mm stream (169) produced a median particle size of 1700 microns, and the 10 mm stream (176) produced a median particle size of 1200 microns. Further stream diameter reduction would be expected to decrease median particle size, if everything else remained constant.

Decreasing tap temperature reduces median particle size. Ht. No. 168 tapped at 2910^oF. All other factors remained constant. Particle size control via tap temperature is not considered good practice since the temperature variable should be reserved for control of powder chemistry.

The effect of metal chemistry on particle size distribution is demonstrated by data for Ht. Nos. 169, 170, and 171. Median particle sizes were 1700 μ , 2150 μ , and 2800 μ respectively. This marked increase in successive heats is ascribed to increasing titanium and aluminum levels in the melts. These increasing levels produce an increasing fraction of flake-like particles which are elongated in two directions and thin in the third,

and consequently have an increased "screen size" for a given particle mass. This effect is also seen in the increasing standard deviation with increasing titanium and aluminum melt levels.

Packing density or the ratio of apparent density of powder to true density of the alloy is an important practical consideration when powders are compacted. A low packing density basically results in extrusion or hot isostatic pressing of empty space in the cans of powder used in the compaction step. Flake-like powders (such as IN-100, Figure 1) may have packing densities as low as 0.3. The packing density of separate size fractions of maraging steel, Ht. No. 148, is presented in Table IV. Overall packing density of a mesh range of -3 1/2/+35 would be $\approx .58$. This value insures efficient use of can space in compaction operations.

Microstructure of powder particles was evaluated routinely. Samples of selected powders were forwarded to MIT for more comprehensive analysis of secondary dendrite arm spacing, solidification structure, and segregation. In the case of maraging steel, the atomization process was found to generate a dispersion of oxides in the particles which varied with particle size. The nature of these dispersions are shown for Ht. No. 172 in Figures 5 through 8. In general, the smaller the size fraction the greater the amount of the dispersed oxide phase. The origin of these oxides is currently under further close study.

C. Heat Treatment Response

With maraging steel coarse powder, an evaluation of the effects of the powder making process on alloy content and uniformity can be carried out by measuring the hardening response of heat treated powder particles. Since the powder particles have "cast" structures, a high temperature homogenization treatment must be used before aging. The heat treatments used were standard for cast 17% Ni maraging steel.¹ Results of these studies are presented in Table V. The effect of homogenization at 2100°F is shown for Ht. No. 166 where the aged Rc hardness increased 4.3 points after the high temperature treatment. The heat treated powder particles do not, in general, harden to the specification for the alloy which is Rc 52/55. Extruded bar stock, Ht. No. 148, was also tested and hardened to Rc 47.0. Possible cause for this low hardness level is discussed in a later section

¹R. F. Decker, C.J. Novak, and T.W. Landig. Journal of Metals, November 1967, p.64

on chemistry. In a series of three heats, 169, 170, and 171, where low tap temperature and titanium and aluminum additions were used (170 and 171) the hardening response of powder approaches the specification for the alloy. Heat treatments were carried out in air and only coarse particles were not completely oxidized. In the case of Ht. No. 171, sizes ≥ 8 mesh were flake so that the 2100°F solution treatment had to be limited to 1 hr. for the 8 mesh size used. The chemistry of this series is discussed in a later section. Finally, the coarse powder of Ht. No. 172 showed the best hardening response of all heats made with no extra alloy additions. This heat was also atomized using improved tundish practice and atomization conditions.

D. Cleaning

Coarse powder maraging steel by steam, argon or nitrogen atomization has a black oxide surface due to reaction with either the atomization fluid or the water in the quench tank used to catch the powder. Figure 4 shows the original oxide coat and also the powder in the clean condition. Removal of oxide was done chemically using the following process:

1. Soak atomized powder in water solution of $\text{NaOH}/\text{KMnO}_4$ (Diversey D-299 commercial preparation) @ 1 lb/gallon concentration @ $180\text{-}200^{\circ}\text{F}$, 1 hr. minimum at temperature.
2. Rinse in water in barrel tumbler, slow tumbling speed.
3. Tumble in inhibited hydrochloric acid in barrel tumbler, slow tumble speed 1/2 hr. minimum (50% Diversey "Everite" + 50% H_2O).
4. Tumble rinse in water, slow tumble speed.
5. Recycle through steps 1-4, 2 to 5X.
6. Dry.
7. Hydrogen reduce tarnish picked up in drying. 1600°F , 1/2 hr. at temperature. Cool to room temperature in dry hydrogen.

This process successfully removed surface oxide and produced clean powder as shown in Figure 4. Oxygen chemistry as a function of cleaning steps is shown in Table II and discussed in the following section.

E. Chemistry

Oxidizing media in the form of steam (atomization) and water (quench in steam and argon atomization) have dictated close attention to oxygen chemistry in maraging steel coarse powder. The results of all oxygen analyses run to date are presented in Table II. Several facts may be noted.

The melting procedure with use of an argon inert gas cover maintained melt oxygen generally in the 20 to 40 ppm range. Significant oxygen increase occurred, however, in the powder with smaller particle sizes showing higher oxygen levels. This may be noted by comparison of "large" and "small" particle values in Ht. Nos. 147, 148, and 167. In Ht. No. 172 (argon atomization) -4/+5 and -16/+48 mesh sizes were analyzed to better define the oxygen pick-up problem. In this case, comparison may be made with Figures 5 and 7 which show oxide inclusions corresponding to 630 ppm (-4/+5 mesh) and 2800 ppm (-16/+18 mesh) oxygen levels. The 630 ppm oxygen is the lowest level observed to date in a coarse powder fraction.

The effect of cleaning cycles on oxygen content was studied for Ht. No. 147. A minor decrease in oxygen level was noted for large particles after more than one cleaning cycle.

Metal chemistry was also followed closely. Results of all analyses obtained to date are presented in Table III.

Oxygen pick-up in melting and atomization was accompanied by titanium and aluminum losses. Whereas the exact strengthening mechanism of aluminum in maraging steels has not been identified, titanium strengthening is ascribed to Ni_3Ti ¹ or FeTi ² sigma phase precipitates. Loss of titanium by oxidation would lead, therefore, to a decrease in the strength which could be developed in the alloy.

¹Banerjee, B. R.; Capenos, J. M.; and Hanser, J. J. *Advances in Electron Metallography* Vol. 6, ASTM STP 396, ASTM 1966, pp 115-131.

²Chilton, J. M.; and Barton, C. J.: *Trans. ASM*, Vol. 60, 1967, pp 528-542.

Analysis of melt dip samples showed that aluminum losses were significant but titanium levels were maintained fairly well under inert gas during melting. Final powder titanium and aluminum levels indicated substantial losses. This may be noted for all coarse powders analyzed. In the melt series 169, 170, and 171, additions were made (see Table I) to the melt just before tap. (169 reference; 170 and 171 contained additions). These higher levels are reflected in melt dip analyses (See Table) but again losses occurred. The ratio of losses in the tundish to those in atomization is not yet determined. Data from Ht. No. 173 where the tundish stream was sampled should provide more information. It should be noted that in Ht. No. 171 the powder titanium level of .48% approaches the spec level of 0.6% for Vascomax 300. The hardening response of powder from this heat was also encouraging (see Table V). The general problem of composition control in coarse powder atomization is under careful study.

F. Powder Consolidation

The intent of the program is to control structure and properties of alloys through a powder metallurgy approach. Once satisfactory powders are obtained, comparison of properties resulting from direct extrusion, hot isostatic pressing and hot isostatic pressing plus extrusion will be carried out. To provide material for initial work in this area by Task IV, extrusion of "state of the art" coarse powders of maraging steel Vascomax 300 was carried out.

Chemically cleaned and hydrogen annealed -4/+35 mesh coarse powders of Ht. Nos. 147 and 148 were sealed in evacuated mild steel cans and extruded under the following conditions:

Can	3 1/2" O.D. x 3.310" I.D.
Liner	3.625" ϕ
Die	1.120" Dia.
Red. Ratio	10.5X
Tooling Temperature	800°F
Billet Temperature	2050°F

Sound 1" ϕ core material was produced in each case and material forwarded to MIT

for property determination.

In the case of IN-100, a preliminary study of hot isostatic pressing conditions was carried out using fine powder produced by Homogeneous Metals. Small compacts were pressed at 2000 and 2300°F @ 25,000 psi for 2 hours. The structure of these compacts after solution treatment at 2200°F is shown in Figures 9 - 12. Several

features may be noted. Prior particle boundaries still exist in both the 2000 and 2300°F pressings. Grain growth has occurred within particles but the 2200°F solution anneal has not brought the 2000°F pressing grain size up to that of the 2300°F pressing with a 2200°F anneal. The conclusion here is that the 2300°F pressing cycle essentially

determined the grain size in that case. Figure 10 shows that the "cast" powder particle structure has not been totally homogenized with the pressing cycle and a 2200°F, 4 hr. solution treatment. The significant impact of the powder approach in producing homogeneous structures of a complex nickel base alloy is clearly apparent here when a

comparison of Figure 10 and Figure 3 is made and it is noted that the dimensional scale of segregation is a full order of magnitude greater for the 3" ϕ cast bar. A practical solution treatment cycle for homogenization of the 3" ϕ section simply could not be devised. The pressing cycle of 2300°F followed by 2200°F, 4 hrs., Figure 12, has fully homogenized the structure with the exception of particle and grain boundary carbides. In both the 2000 and 2300°F pressings, Figures 10 and 12, grain growth appears to be controlled by grain and particle boundary carbides. This behavior is under further study because of implications with respect to high temperature properties of the IN-100 alloy.

Ht. No.	Extrusion Force	Ram Speed
147	535 tons upset, 500 tons running	130-165"/min.
148	565 tons upset, 535 tons running	80-130"/min.
147 & 148 (blend)	535 tons upset, 500 tons running	160-180"/min.

Melting and Atomization

Median Particle Size Microns.
Standard Deviation = 84% Point/50% Point

Nozzles, Pressures

Heat No.	Alloy	Weight Lbs.	Atomization Steam, Argon, Nitrogen	Nozzles, Pressures		Tundish Nozzle	Tap Temperature	Objective	Result	Median Particle Size Microns. Standard Deviation = 84% Point/50% Point
				Top Pressure	Side Pressure					
136	VM-300	13.4	S	60 mmg 8 psig	2.5 x 100 mmf 10 psig	10 mm	3200	Preliminary test of VM-300 atomization.	Coarse rounded powder. Oxidized.	1650; σ = 2.18
137	VM-300	13.0	Ar	-	Unijet "U" 50 psig	10 mm	3150	Preliminary test of VM-300 atomization.	Coarse rounded powder. Oxidized.	2330; σ = 1.48
145	VM-300	17.2	S	60 mmg 9 mmg	2.5 x 100 mmf 12 psig	10 mm	3040	Test reduced tap temp.	Coarse rounded powder. Tundish freeze up.	1700; σ = 1.94
146	VM-300	16.2	S	60 mmg 9 psig	"	11.9 mm	3035	Test increased tundish nozzle to reduce freeze-up.	Coarse rounded powder. Freeze up of last ~ 3 lbs. in tundish.	2000; σ = 1.85
147	VM-300	34.0	S	"	"	"	3090	Produce material for cleaning and extrusion.	Coarse rounded powder. Oxidized.	2050; σ = 1.90
148	VM-300	34.2	S	"	"	"	3080	Produce material for cleaning and extrusion.	Coarse rounded powder. Oxidized.	2250; σ = 1.91
149	IN-100	22.1	S	"	"	"	3070	Preliminary test of IN-100 atomization.	Sharp flaky powder. Thin adherent oxide.	Not determined.
150	VM-300	33.9	S	"	"	"	3060	Produce material for hot isostatic pressing and extrusion.	Coarse rounded powder. Oxidized.	2000; σ = 1.95

Table 1

Melting and Atomization

Heat No.	Alloy	Weight Lbs.	Atomization Steam, Argon, Nitrogen	Nozzles, Pressures			Tundish Nozzle	Tap Temperature	Objective	Result	Median Particle Size Microns. Standard Deviation = 84% Point/50% Point
				Top Pressure	Side Pressure	Tap Temperature					
151	VM-300	33.8	S	60 mmg 9 psig	2.5 x 100 mmf 12 psig	11.9 mm	3095	Produce material for hot isostatic pressing and extrusion.	Coarse rounded powder. Oxidized.	151, 152, 153 combined heats:	
152	VM-300	33.8	S	"	"	"	3110	"	"	2350; $\sigma = 1.92$	
153	VM-300	33.9	S	"	"	"	3085	"	"		
166	VM-300	17.0	S	"	"	12.7 mm	2870	Test effect of lower tap temperature on losses of Ti and Al.	Coarse rounded powder. Black oxide coat.	Not determined.	
167	VM-300 + 0.25% Al, 0.30% Ti	17.0	S	"	"	"	2900	Test recovery of late melt additions of Ti and Al.	Coarse rounded powder. Black oxide coat. See Tables II, III.	Not determined.	
168	VM-300	17.2	S	"	"	"	2910	Test tap temp. of 2750°F.	Temperature overshoot. Tapped @ 2910. Coarse rounded powder.	2000; $\sigma = 1.90$	
169	VM-300	16.9	S	"	"	"	2760	Test effect of lower tap temp. on losses of Ti and Al.	Rounded powder. Black oxide coat. See Tables II, III.	1700; $\sigma = 1.88$	
170	VM-300 + 0.06% Al 0.74% Ti	17.0	S	"	"	"	2775	Test recovery of Ti and Al additions with low tap temperature.	Coarse rounded powder. Larger particles elong- ated. See Tables II, III.	2150; $\sigma = 2.21$	

Table I

Melting and Atomization

Median Particle Size Microns.
Standard Deviation = 84% Point/50% Point

Heat No.	Alloy	Weight Lbs.	Atomization		Nozzles, Pressures		Tundish	Top Temperature	Objective	Result	Median Particle Size Microns. Standard Deviation = 84% Point/50% Point
			Argon, Steam, Nitrogen	Top Pressure	Side Pressure	Top Pressure					
171	VM-300+ 0.09% Al 1.10% Ti	17.0	S	60 mmg 9 psig	2.5 x 100 mmf 12 psig	12.7 mm	2765	Test recovery of Ti and Al additions with low tap temperature.	Small fractions rounded. Large particles flake-like. See Tables II, III.	2800; σ = 2.50	
172	VM-300	25.2	Ar	-----	Unijet "U" 60 psig	10 mm	2845	Test improved tundish practice and argon atomization on oxygen pick-up. Ti, Al recovery.	Coarse rounded powder. Black oxide coat. See Tables II, III.	3100; σ = 2.06	
173	VM-300	25.2	Ar	-----	Unijet "U" 70 psig	"	2830	Reduce size range. Test oxygen pick-up, and Ti, Al recovery. Sample liquid metal stream out of tundish.	Coarse rounded powder. Black oxide coat. Chemistry results not back at report time.	2350; σ = 1.70	
174	VM-300	25.5	N ₂	-----	Unijet "U" 70 psig	"	2815	Test N ₂ atomization on oxygen pick-up and Ti, Al recovery.	Coarse rounded powder. Black oxide coat. Chemistry results not back.	1750; σ = 2.17	
175	IN-100	22.8	Ar	-----	Unijet "U" 60 psig	"	2650	Test Argon atomization of IN-100 with improved tundish practice.	Sharp pointed, twisted flakes.	Not determined.	
176	VM-300	26.6	S	60 mmg 9 psig	2.5 x 100 mmf 12 psig	"	2790	Test steam atomization on oxygen pick-up and Ti, Al recovery with improved tundish practice.	Medium rounded powder. Black oxide coat. Chemistry results not back.	1200; σ = 2.0	

Table II

Oxygen Chemistry

Heat No.	Alloy	Sample Description	Result (ppm)
147	VM-300	1. Melt dip sample (all melt samples taken just before tap).	37
		2. Coarse powder, 1 chemical cleaning cycle. "Large" particles. "Small" particles.	1500
		3. Coarse powder, 2 chemical cleaning cycles. "Large" particles. "Small" particles.	1500
		4. Coarse powder, 3 chemical cleaning cycles. "Large" particles. "Small" particles.	990
		5. Coarse powder, 3 chemical cleaning cycles + 1600°F Hz reduction. "Large" "Small"	1200
		6. Duplicate analysis of (5) "Large" "Small"	1500
		7. Extruded bar; center of extrusion length.	1000
148	VM-300	1. Melt dip sample.	1600
		2. Coarse powder, 3 chemical cleaning cycles + 1600°F Hz reduction. "Large" "Small"	2000
		3. Duplicate analysis of (2).	1500
		4. Extruded bar; center of extrusion length.	20
150	VM-300	1. Melt dip sample.	900
		1. Melt dip sample.	1400
		1. Melt dip sample.	710
		1. Melt dip sample.	1100
151	VM-300	1. Melt dip sample.	1400
		1. Melt dip sample.	19
		1. Melt dip sample.	28
		1. Melt dip sample.	50
152	VM-300	1. Melt dip sample.	26
		1. Melt dip sample.	
		1. Melt dip sample.	
		1. Melt dip sample.	

Table II

Oxygen Chemistry

Heat No.	Alloy	Sample Description	Result (ppm)
166	VM-300	1. Melt dip sample.	14
		2. Coarse powder, -4/+14 mesh. 1 chemical cleaning cycle.	1800
		3. Coarse powder, -14 mesh. 1 chemical cleaning cycle.	1600
167	VM-300	1. Melt dip sample.	2400
		2. Coarse powder, -4/+14 mesh. 1 chemical cleaning cycle.	36
		3. Coarse powder, -14 mesh. 1 chemical cleaning cycle.	1100
168	VM-300	1. Melt dip sample.	950
		2. Coarse powder, -4/+14 mesh. 1 chemical cleaning cycle.	2200
		3. Coarse powder, -14 mesh. 1 chemical cleaning cycle.	37
169	VM-300	1. Melt dip sample.	1800
		2. Coarse powder, -14 mesh. 1 chemical cleaning cycle.	13
170	VM-300	1. Melt dip sample.	2400
		2. Coarse powder, -14 mesh. 1 chemical cleaning cycle.	24
171	VM-300	1. Melt dip sample.	2500
		2. Coarse powder, -14 mesh. 1 chemical cleaning cycle.	28
172	VM-300	1. Melt dip sample.	2400
		2. Coarse powder, -14 mesh. 1 chemical cleaning cycle.	21
		3. Coarse powder, -16/+18 mesh. 2 chemical cleaning cycles. Final HCl etch.	630
		3. Coarse powder, -16/+18 mesh. 2 chemical cleaning cycles. Final HCl etch.	2800

Table IV

Packing Density
Maraging Steel Coarse Powder

Heat No. 148

<u>Mesh</u>	<u>Packing Density</u>
-3 1/2/+4	.56
-4/+5	.58
-5/+6	.55
-6/+7	.56
-7/+8	.56
-8/+10	.58
-10/+12	.59
-12/+14	.60
-14/+16	.60
-16/+18	.60
-18/+20	.58
-20/+25	.56
-25/+30	.56
-30/+35	.42

Heat Treating Response - Maraging Steel Coarse Powder

Heat No.	Sample Description	Heat Treatment	Hardness Rc
1404-A	1 3/4" ϕ bar. Mill certification.	900°F - 3 hrs.	53.8
143	1. Melt dip sample.	1500°F, 1/2 hr. A.C. + 900°F, 3 hr.	46.5
166	2. Extrusion of 148 coarse powder.	1500°F, 1/2 hr. A.C. + 900°F, 3 hr.	47.0
167	1. + 3 1/2 mesh (6 mm) particles.	900°F, 3 hrs.	44.0
167	2. + 3 1/2 mesh (6 mm) particles.	2100°F, 4 hrs. A.C., + 900°F, 3 hrs.	48.3
167	1. + 3 1/2 mesh (6 mm) particles.	900°F, 3 hrs.	46.1
167	2. + 3 1/2 mesh (6 mm) particles.	2100°F, 4 hrs. A.C., + 900°F, 3 hrs.	50.7
168	1. + 4 mesh (5 mm) particles.	2100°F, 1 hr. A.C., + 900°F, 3 hrs.	47.9
168	2. + 4 mesh (5 mm) particles.	2100°F, 4 hrs. A.C., + 900°F, 3 hrs.	48.4
169	1. + 4 mesh (5 mm) particles.	2100°F, 1 hr. A.C., + 900°F, 3 hrs.	48.5
169	2. + 4 mesh (5mm) particles.	2100°F, 4 hrs. A.C., + 900°F, 3 hrs.	48.6
170	1. + 4 mesh (5 mm) particles.	2100°F, 1 hr. A.C., + 900°F, 3 hrs.	50.3
170	2. + 4 mesh (5 mm) particles.	2100°F, 4 hrs. A.C., + 900°F, 3 hrs.	52.2
171	1. 8 mesh (2 mm) particles.	2100°F, 1 hr. A.C., + 900°F, 3 hrs.	51.6
172	1. + 4 mesh (5 mm) particles.	900°F, 16 hrs. A.C.	46.2
172	2. + 4 mesh (5 mm) particles.	2100°F, 2 hrs. A.C., + 900°F, 3 hrs.	49.3

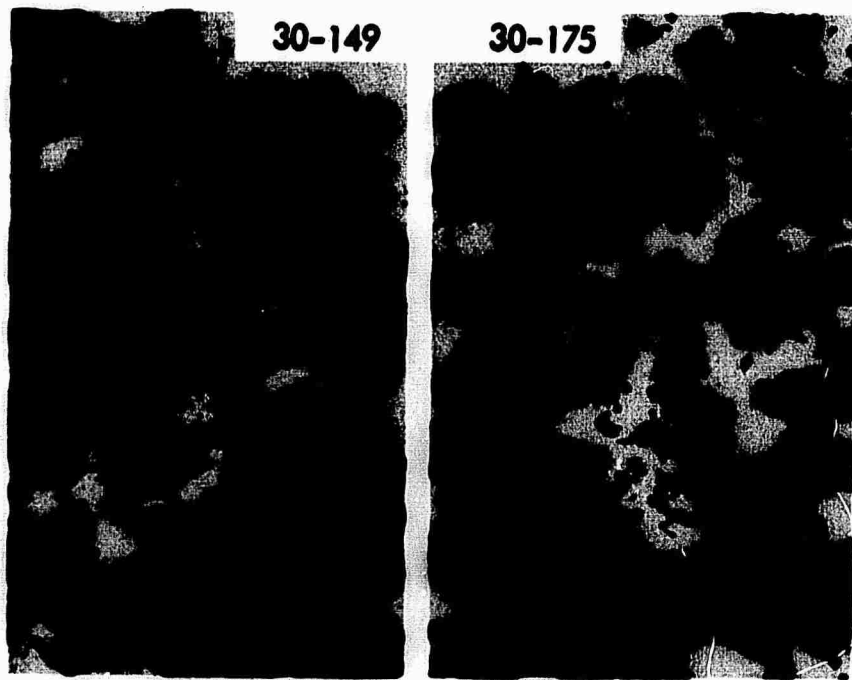


Figure 1. IN-100. Heat No. 149, as atomized, steam; Heat No. 175, as atomized, argon. 1X.

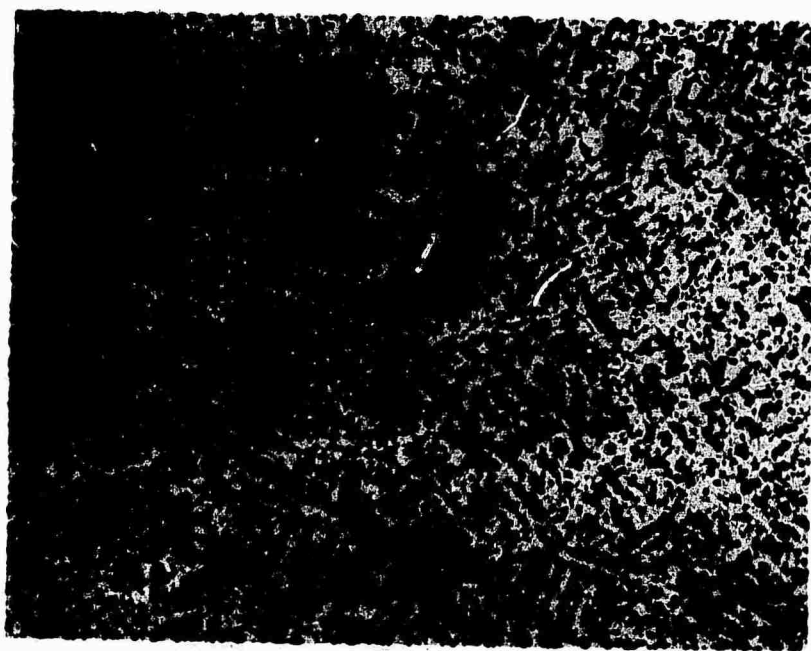


Figure 2. IN-100. Heat No. 149. -3 1/2/+4 mesh.
Powder particle dendrite structure. Etched, 200X.

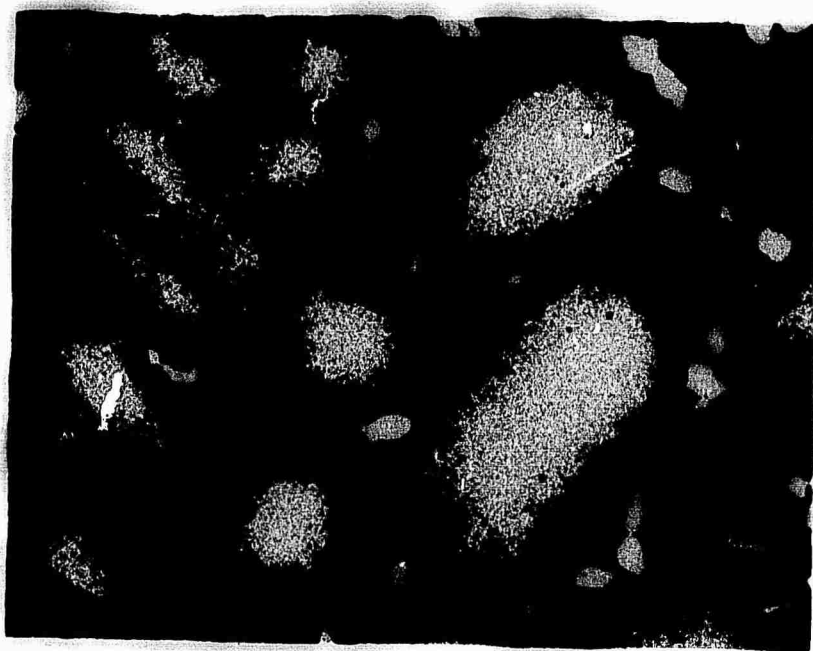


Figure 3. IN-100. Three inch diameter cast bar. Solidification structure. Etched, 200X.

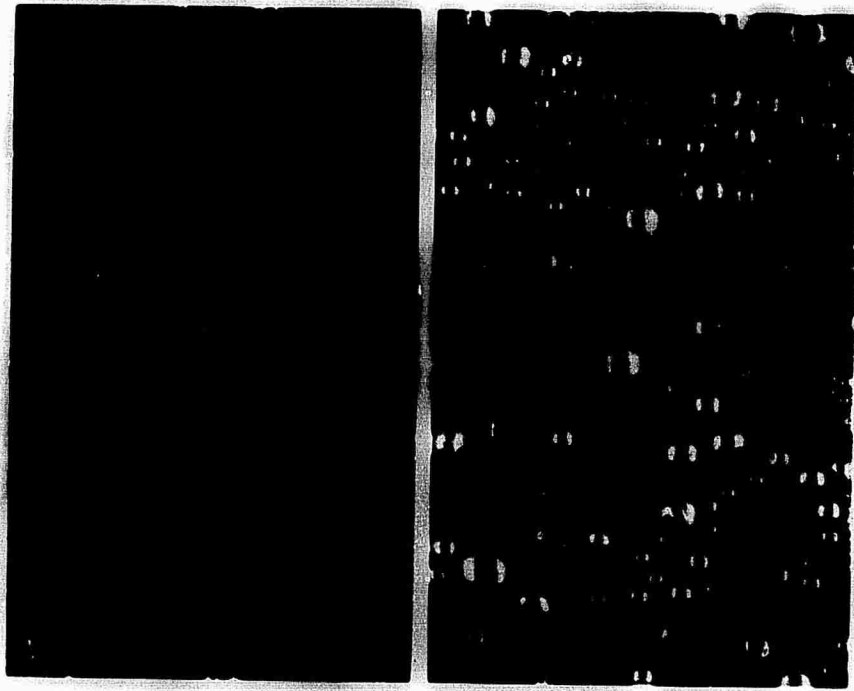
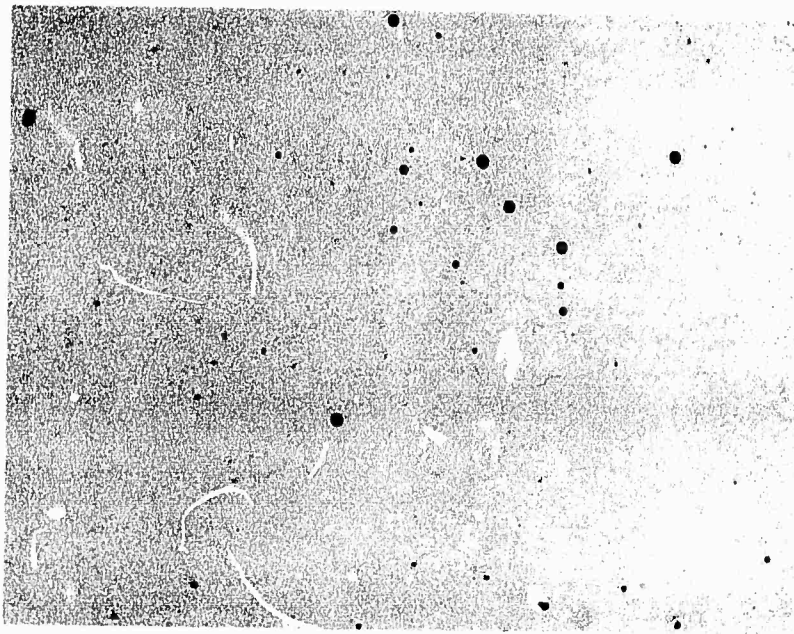
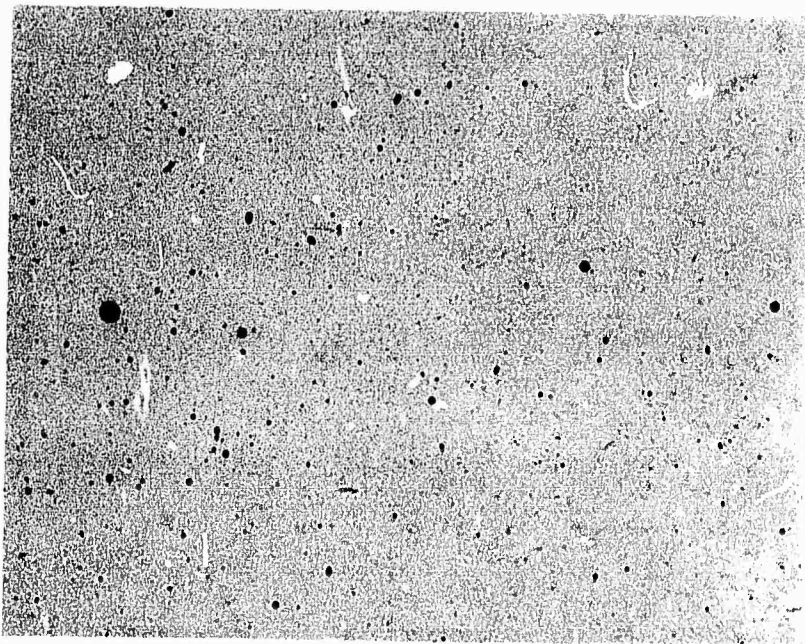


Figure 4. Vascomax 300. Heat No. 148, as atomized, left; cleaned, right. 1X.



**Figure 5. Vascomax 300. Heat No. 172. -4/+5 mesh particles.
Fine oxide dispersion. Unetched, 1000X.**



**Figure 6. Vascomax 300. Heat No. 172. -8/+10 mesh particles.
Fine oxide dispersion. Unetched, 500X.**

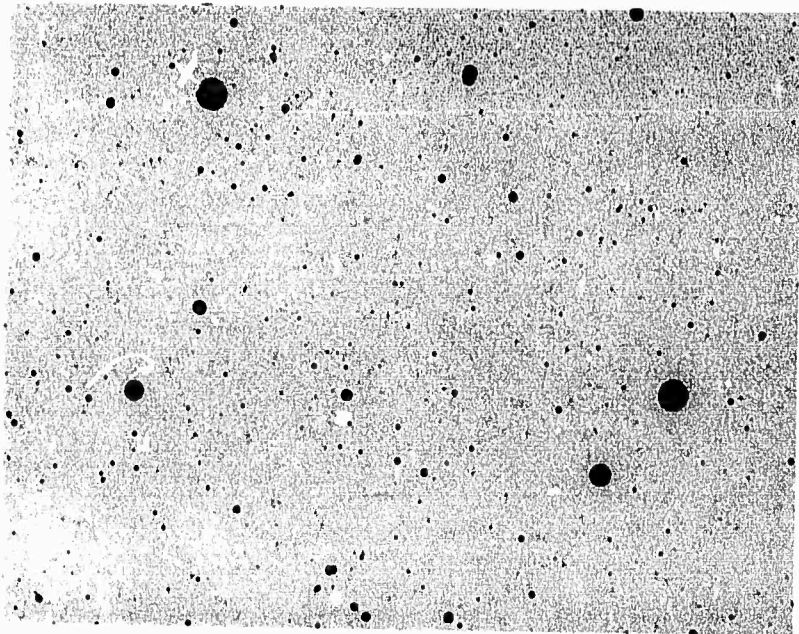


Figure 7. Vascomax 300. Heat No. 172. -16/+18 mesh particles. Oxide dispersion. Unetched, 500X.

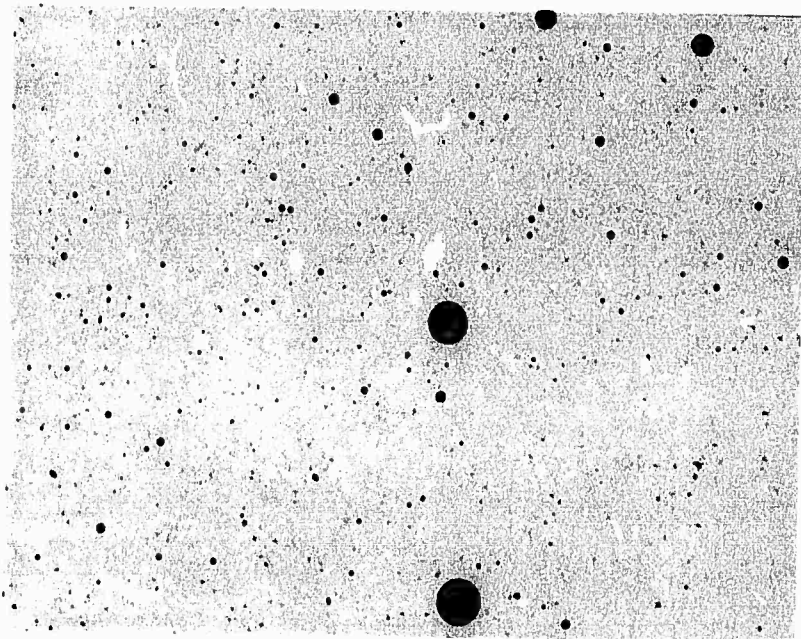


Figure 8. Vascomax 300. Heat No. 172. -25/+30 mesh particles. Oxide dispersion. Unetched, 500X.

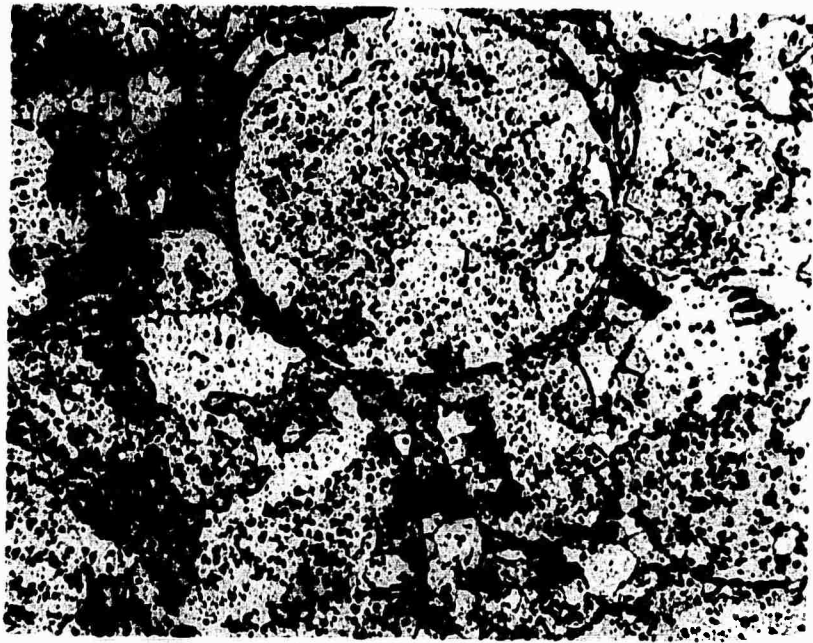


Figure 9. IN-100. Homogeneous Metals -20 mesh powder. Hot isostatically pressed 2000°F, 25,000 psi, 2 hours. Solution treated 2200°F, 4 hours, W.Q. Etched, 100X.

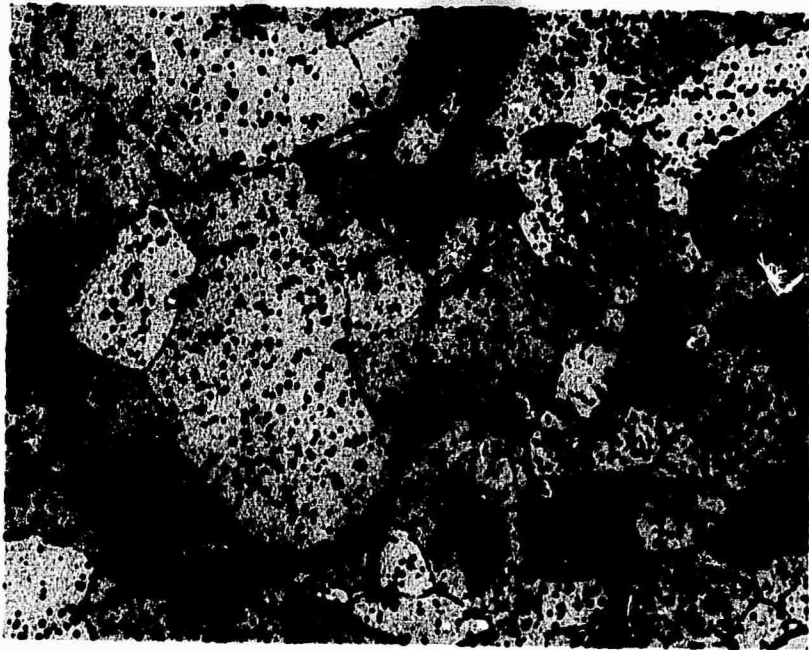


Figure 10. Same structure as Figure 9. 500X.

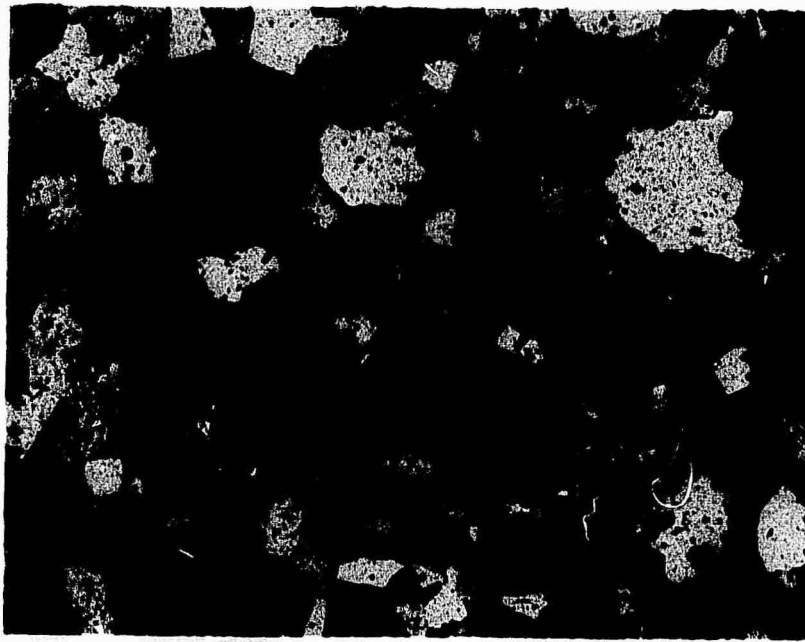


Figure 11. IN-100. Homogeneous Metals -20 mesh powder. Hot isostatically pressed 2300° F, 25,000 psi, 2 hours. Solution treated 2200° F, 4 hours, W.Q. Etched, 100X.

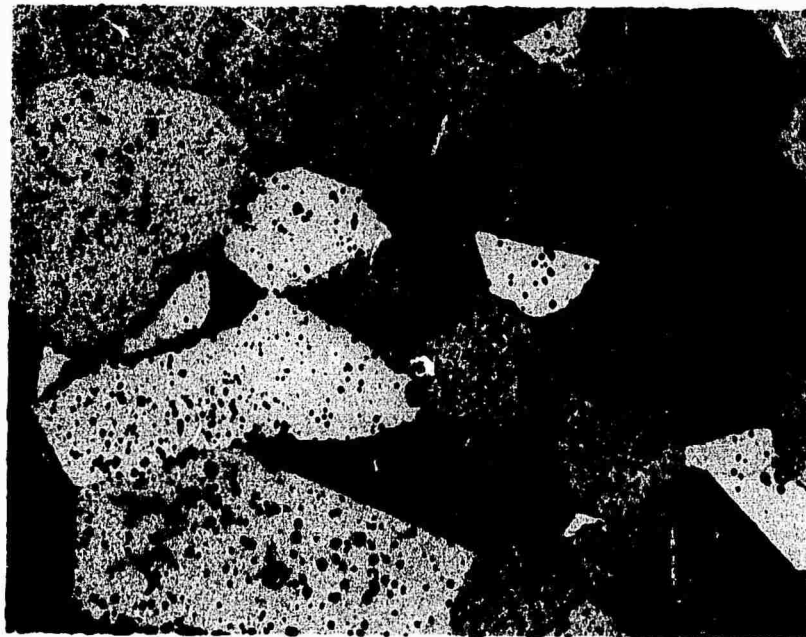


Figure 12. Same structure as Figure 11. 500X.

MAUFFEL & ESSER CO.

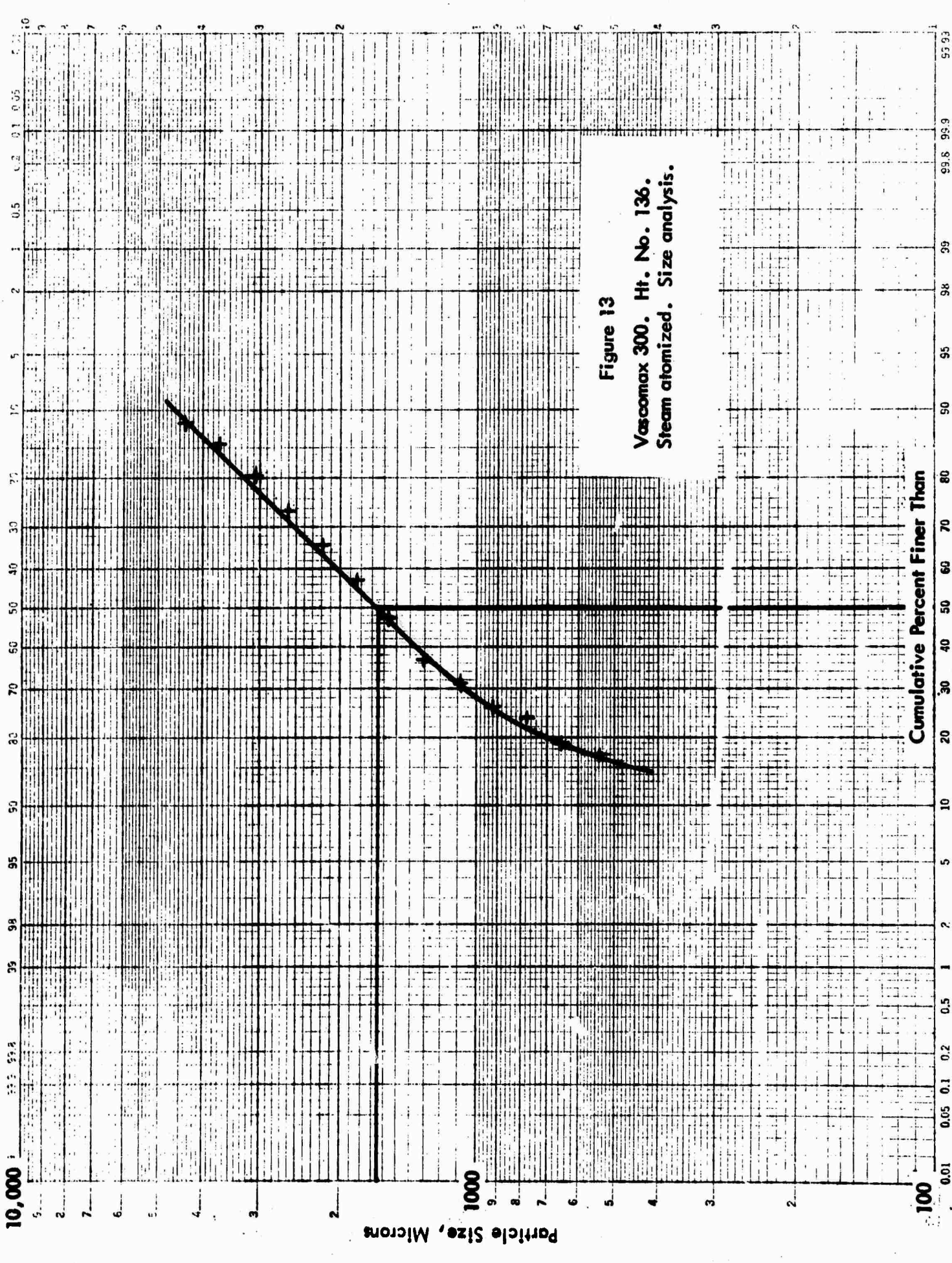


Figure 13
Vascomax 300. Ht. No. 136.
Steam atomized. Size analysis.

TASK II - SOLIDIFICATION RESEARCH

by

P. A. Joly
R. G. Riek
R. Mehrabian
M. C. Flemings

ABSTRACT

The effect of a wide range of cooling rates (0.1 to 10^5 °C/sec) on the dendritic structure of maraging 300 alloy is determined, and the relationship $d = 39\epsilon^{-0.25}$ between secondary dendrite arm spacing, d , and cooling rate, ϵ , is established. Structures of atomized particles of maraging 300 alloy, received from IMT, are presented and corresponding cooling rates during atomization are estimated from the relationship above. A simple heat flow analysis is proposed that will facilitate calculation of solidification times during atomization:

Finally, a laboratory apparatus for rapid solidification of metallic alloys is described and corresponding structures of cast maraging 300 alloy are presented.

INTRODUCTION

In the first six months of this program, Task II (solidification group) has conducted research on heat flow and microsegregation of maraging 300 alloy. The general aim of the program has been the study of heat flow and structure of the atomized particles (flakes, droplets, pellets) produced at IMT, and the development of new methods of rapidly solidifying small to medium-size pellets of metal alloys. Specific aspects of the work have included:

1. Determination of the relationship between cooling rate and secondary dendrite arm spacing for maraging 300 alloy.
2. Detailed study of heat flow and structure of atomized particles of maraging 300 alloy produced at IMT.
3. Development of small scale laboratory apparatus for rapid solidification of small to medium-size droplets or rods of metal alloys.

1. EFFECT OF COOLING RATE ON STRUCTURE OF MARAGING 300 ALLOY

Cooling rate during solidification has a pronounced effect on cast structures, particularly on fineness of dendrite structure and of associated inclusions and micro-porosity. In order to ascertain the influence of processing

variables on cooling rates and solidification structures of maraging 300 alloy, the following study was undertaken.

The effect of cooling rate on secondary dendrite arm spacing over a wide range of cooling rates, $0.1^{\circ}\text{C}/\text{sec}$ to $10^{50}\text{C}/\text{sec}$, was determined. The various cooling rates were obtained by levitation melting and casting of small droplets (1 to 2 grams), unidirectional solidification of a 2.5 Kg. ingot, and vacuum melting of 700 grm charge in an alumina crucible and furnace cooling.

Levitation Melting and Casting

Figure 1 is a sketch of the levitation melter and associated apparatus. The details of this apparatus have previously been described(1). Droplets of the maraging 300 alloy were levitated inside the glass tube in an atmosphere of helium. The temperature of the droplets were continuously monitored using a two-color optical pyrometer. The molten levitated droplets were solidified and cooling rates measured using the following techniques:

(a) Gas Quenching. With sufficiently high flow rates of hydrogen or helium, droplets were solidified while levitated. Measured cooling rates, via the two-color optical pyrometer were of the order of $1 - 15^{\circ}\text{C}/\text{sec}$.

(b) Oil Quenching. Somewhat higher cooling rate was obtained by liquid quenching. The liquid quench tank was

placed where the splat cooler is shown in Figure 1; the power to the levitation coil was turned off, and the charge dropped through the plastic seal into the liquid. A cooling rate of $140^{\circ}\text{C}/\text{sec}$ has been calculated for oil quenching(2).

(c) Chill Casting. Chill castings in a copper mold with plate shaped mold cavity of 0.08" thickness, inserted in the turntable in the enclosure in Figure 1, were made and cooling rates on the order of $10^{30}\text{C}/\text{sec}$ were measured as previously described.(1)

(d) Splat Cooling. Maximum cooling rates (on the order of $10^{50}\text{C}/\text{sec}$) were obtained using the hammer and anvil type splatter shown in Figure 1. The details of this technique have again been described elsewhere(1).

Unidirectional Casting

A 2" by 2" by 5" tall unidirectional ingot of maraging 300 was cast using a composite mold of CO_2 sand and insulating molding material, fiberchrome. A water-cooled stainless steel chill was located at the base opening of the mold. Thermal measurements were made by utilization of four Pt-Pt/10% Rh silica shielded thermocouples located along the length of the ingot mold. Measured cooling rates and secondary dendrite arm spacings at different locations in this ingot are shown in Figure 2.

Vacuum Melting and Furnace Cooling

Several specimens of maraging 300 weighing approximately 700 grams were vacuum melted in an alumina crucible in a Balzer furnace. These samples were solidified inside the crucible by decreasing the power input to the furnace at different rates and temperature profiles were recorded with a Pt-Pt/10% Rh thermocouple inserted in the melt. Results of cooling rates versus dendrite arm spacings are again shown in Figure 2.

The microstructure of maraging 300 alloy is shown qualitatively to be refined by increased cooling rates in Figure 3. Figure 2 is a plot of the secondary dendrite arm spacing versus cooling rates. Secondary dendrite arm spacing varies linearly with cooling rate on this log-log plot over the range of cooling rates studied. Equation of the experimentally determined relationship is:

$$d = 39\epsilon^{-0.25}$$

where d is secondary dendrite arm spacing in microns and ϵ is the cooling rate dT/dt in $^{\circ}\text{C}/\text{sec}$.

2. ANALYSIS OF STRUCTURE AND HEAT FLOW OF ATOMIZED PARTICLES

During the course of this investigation, several batches of atomized coarse powder samples of maraging 300 alloy were received from IMT. A detailed study of the structures coupled

with data developed in the previous section have facilitated a simple heat flow analysis during atomization.

Structure of Atomized Particles

The structures of steam or gas atomized powders were evaluated using fineness of dendritic structure and porosity as criteria. Table 1 shows the different series of coarse powders received from IMT and studied. Figure 4 is a plot of average secondary dendrite arm spacing versus diameter of coarse powders made by both steam and argon atomization.

Study of structures obtained reveal that:

(a) Average secondary dendrite arm spacings increase with increasing size of atomized powders. There is a tendency toward finer dendrite arm spacing as the superheat is lowered, Table 1 and Figure 4. There also seems to be a change in fineness of dendritic structure, hence cooling rates during atomization, depending on the quenching medium. However, this latter trend is not conclusive and further examination of atomized powders is necessary.

(b) In steam atomized coarse powders, heats 30 - 147 and 30 - 148, there is a tendency towards a duplex dendritic structure, see micrographs in Figure 5. The finer dendrites are on the outside layer of the pellets and the coarser on the inside. It appears that these larger pellets were only partially solidified during flight; thus, the finer spacings

on the outside edges of the samples. The coarser structures must have resulted from quenching in the water bath below. The steam formation around each pellet in the water bath must cause a reduction in the heat transfer coefficient; hence the coarser structures.

(c) In general steam atomized powders exhibit a larger amount of gas porosity than argon atomized powders, Figure 6.

Heat Flow During Atomization

Newton's Law of cooling for a spherical droplet with "h controlled" heat transfer is written

$$hA(T - T_0) = C_p \rho V \frac{dT}{dt}$$

where:

- T_0 = medium temperature, °C
- T = temperature of droplet, °C
- A = area of the specimen, cm²
- V = volume of the specimen, cm³
- ρ = density of the specimen, g/cm³
- C_p = specific heat of the specimen, cal/g°C
- h = heat transfer coefficient, radiation plus convection, cal/cm²sec°C
- $dT/dt = \epsilon$ = cooling rate at temperature T , °C/sec.

Using the above expression, a value for the combined heat transfer coefficient of radiation and forced convection during atomization may be calculated from cooling rates

obtained from Figure 2, using measured secondary dendrite arm spacings of atomized droplets. For example, measured secondary dendrite arm spacing of an atomized droplet, of maraging 300 alloy 1 mm in diameter, is about 7 microns, Figure 4. From Figure 2 we can estimate a corresponding cooling rate of 10^3 °C/sec during atomization. Using the values of heat capacity and density, of Fe-25% Ni alloy* and atomization temperature of 1500°C, the value of $h = 0.0095$ cal/cm²sec°C and the Nusselt number $hD/k = 0.0082$ are calculated, where D is the diameter of the droplet. Therefore, heat flow during atomization is "h controlled", since $hD/k \ll 1$.

Solidification times can also be calculated from the information available. Cooling rates of the order of 10^3 °C/sec were obtained in the thin plate chill castings made from molten levitated droplets. These measurements were made by embedding a small Pt-Pt/10% Rh thermocouple (No. 38 wire) in the side of the plate casting. The output was recorded on an oscilloscope giving cooling curves over a temperature range of 1425°C to 1300°C. It is assumed that the rate of heat extraction during solidification is equal to the rate of heat extraction over this temperature range. A heat balance for the "h controlled" heat flow is made and solidification time computed.

* For Fe-25% Ni alloy, the following values have been reported(1,2): $C_p = 0.107$ cal/g°C, $\rho = 8$ g/cm³, Latent heat of fusion, $H = 72$ cal/g, and thermal conductivity, $k = 0.115$ cal/cm.sec°C.

$$q = C_p \rho V \frac{dT}{dt} = H \rho \frac{V}{t_f} \quad (2)$$

where dT/dt is measured cooling rate in the temperature range above, in the solid, and t_f = solidification time, seconds.

$$t_f = \left(\frac{H}{C_p} \right) / \left(\frac{dT}{dt} \right) \quad (3)$$

Using the predicted cooling rate of 10^{30} C/sec for a 1 mm droplet of maraging 300 alloy, a solidification time of $t_f = 0.67$ seconds is calculated from equation (3).

A second method of predicting solidification time theoretically has been outlined in a recent publication by Szekely and Fisher (3). They have considered solidification of a metal droplet due to thermal radiation alone. A very simple asymptotic solution is given, which is valid for the size range of atomized droplets under consideration here. The equations of interest are:

$$2R/D = (1 - Ct)^{1/3} \quad (4)$$

$$C = - \frac{6\sigma E}{DH\rho} [T_e^4 - (T_{mp} + 273)^4] \quad (5)$$

where: R = position of the solidification front, cm

D = diameter of droplet, cm

σ = Boltzmann's constant = 1.35×10^{-2} cal/cm²sec·K⁴

E = total emissivity of the droplet

T_e = temperature of the environment, °K

When $2R/D = 0.28$, 98% of the spherical droplet is solidified. Therefore, we have used this ratio and an emissivity value of 0.5 in our calculations, with all other data same as before.

The calculated value of $C = 0.7 \text{ sec}^{-1}$ and the resulting solidification time $t_f = 1.4$ seconds. This calculated value is twice as large as that estimated from measured dendrite arm spacings and cooling rates. However, considering the fact that only heat flow by radiation is considered here and the uncertainty of the data used, the discrepancy is acceptable.

3. RAPID SOLIDIFICATION OF METAL ALLOYS

In line with the proposal submitted for the first year of this investigation, Task II has been studying the feasibility of new and improved techniques in rapid solidification of small to medium sized droplets of high temperature metallic alloys.

A set of copper chill molds were designed and constructed to fit in our Balzer vacuum furnace. Figure 7 shows a section of the mold used in casting of rapidly solidified maraging 300 alloy rods of $5/16"$ by $5/16"$ by 5" long. The structures of these rods were examined in detail and secondary dendrite arm spacings measured. Figure 8 shows the structure of these rapidly solidified rods, while Figure 9 shows the measured secondary dendrite arm spacings along the small dimension of the rods. Our results show that these castings exhibit

dendrite arm spacings consistently less than 15 microns. These fine structures are quite comparable to coarse powder structures obtained from the atomization process.

It is quite conceivable that a continuous production of rapidly solidified rods of high temperature metallic alloys may be an alternative method of obtaining initial, fine structured, material for subsequent hot isostatic pressing into large billets. In line with this approach, a set of rods of maraging 300 alloy, vacuum cast in our laboratory were forwarded to IMT for hot-isostatic pressing into a small billet. Further segregation studies will be carried out on this billet.

Finally, an electroslag remelting apparatus was also constructed to make rapidly solidified rods. Initial experiments have resulted in successful production of 1/2" diameter castings with secondary dendrite arm spacings less than 15 microns.

CONCLUSIONS

1. Secondary dendrite arm spacing in maraging 300 alloy varies linearly with cooling rate to an exponent of $- 1/4$.
2. Cooling rates during steam or argon atomization of coarse powders of maraging 300 alloy are in the range of 10^2 to 10^3 C/sec with resulting secondary dendrite arm spacings of 5 to 12 microns, in particles of 0.5 to 4.5 mm in diameter.
3. A continuous production technique of rapidly solidified rods of metallic alloys may be an alternative method of obtaining initial, fine structured, material for subsequent hot-pressing into large billets.

BIBLIOGRAPHY

1. W. E. Brower, Jr., R. Strachan, M. C. Flemings, "Effect of Cooling Rate on Structure of Ferrous Alloys", *Cast Metals Research Journal*, Vol. 6, No. 4 (1970), pp. 176-180.
2. W. E. Brower, Jr., "Solidification-Structure-Fracture Relations in Inclusion Bearing Iron", Ph.D. Thesis, Department of Metallurgy and Materials Science, Massachusetts Institute of Technology (1969).
3. S. Szekely and R. S. Fisher, "On the Solidification of Metal Spheres Due to Thermal Radiation at the Bounding Surface", *Metallurgical Transactions*, Vol. 1, (1970), pp. 1480-1482.

Table I
Samples of Atomized Coarse Powders
of Maraging 300 Alloy Received from IMT

<u>heat number</u>	<u>tap temperature</u>	<u>atomization</u>	<u>particle size</u>
30-137	3150 ^o F	argon	-4/+5, -12/+14, -14/+30
30-147	3090 ^o F	steam	-4/+5, -8/+10, -16/+18, -25/+30
30-148	3080 ^o F	steam	-4/+5, -8/+10, -16/+18, -25/+30
30-172	2845 ^o F	argon	-4/+5, -8/+10, -16/+18, -25/+30

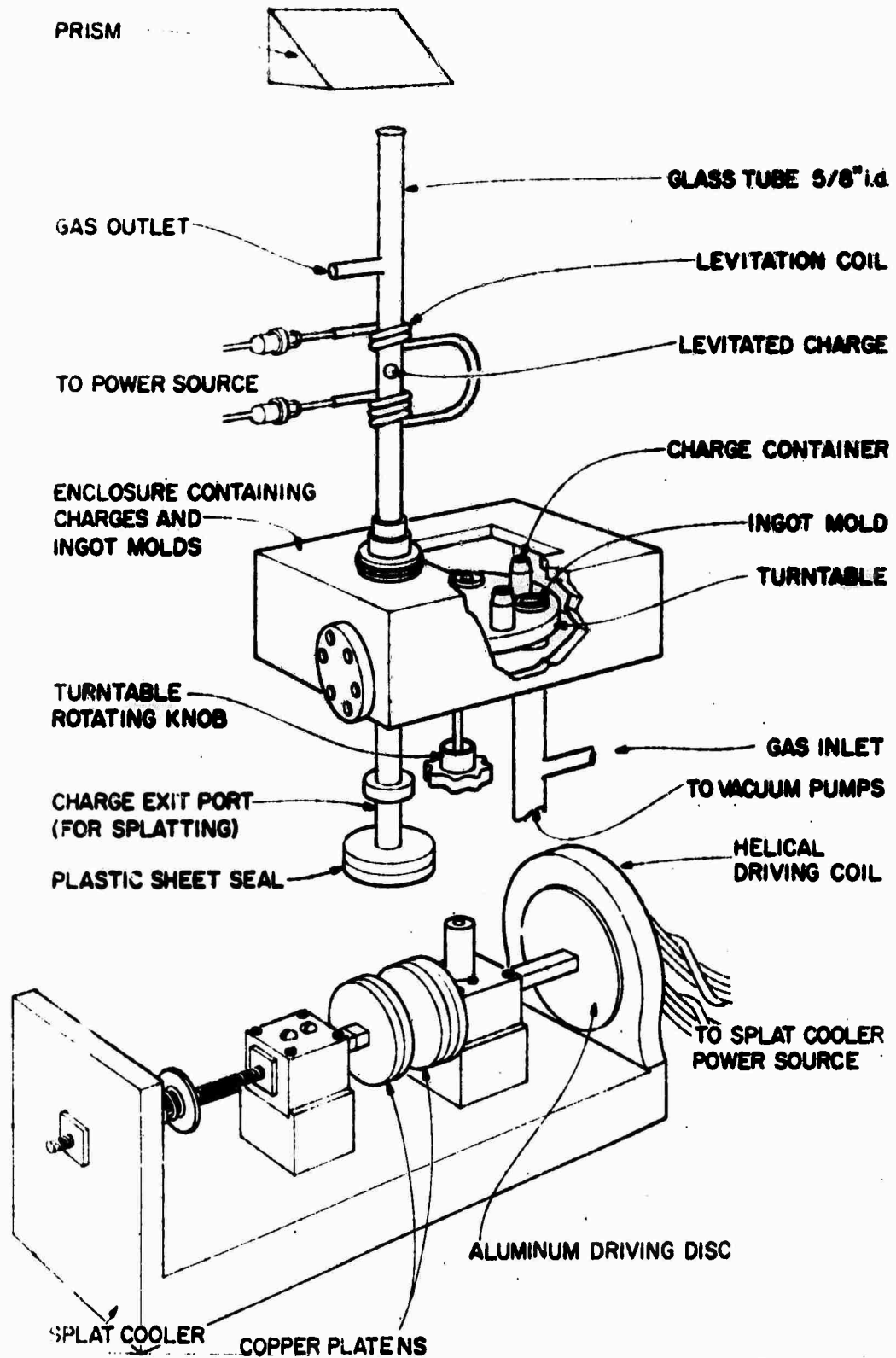


Figure 1. Sketch of levitation melting and casting apparatus.

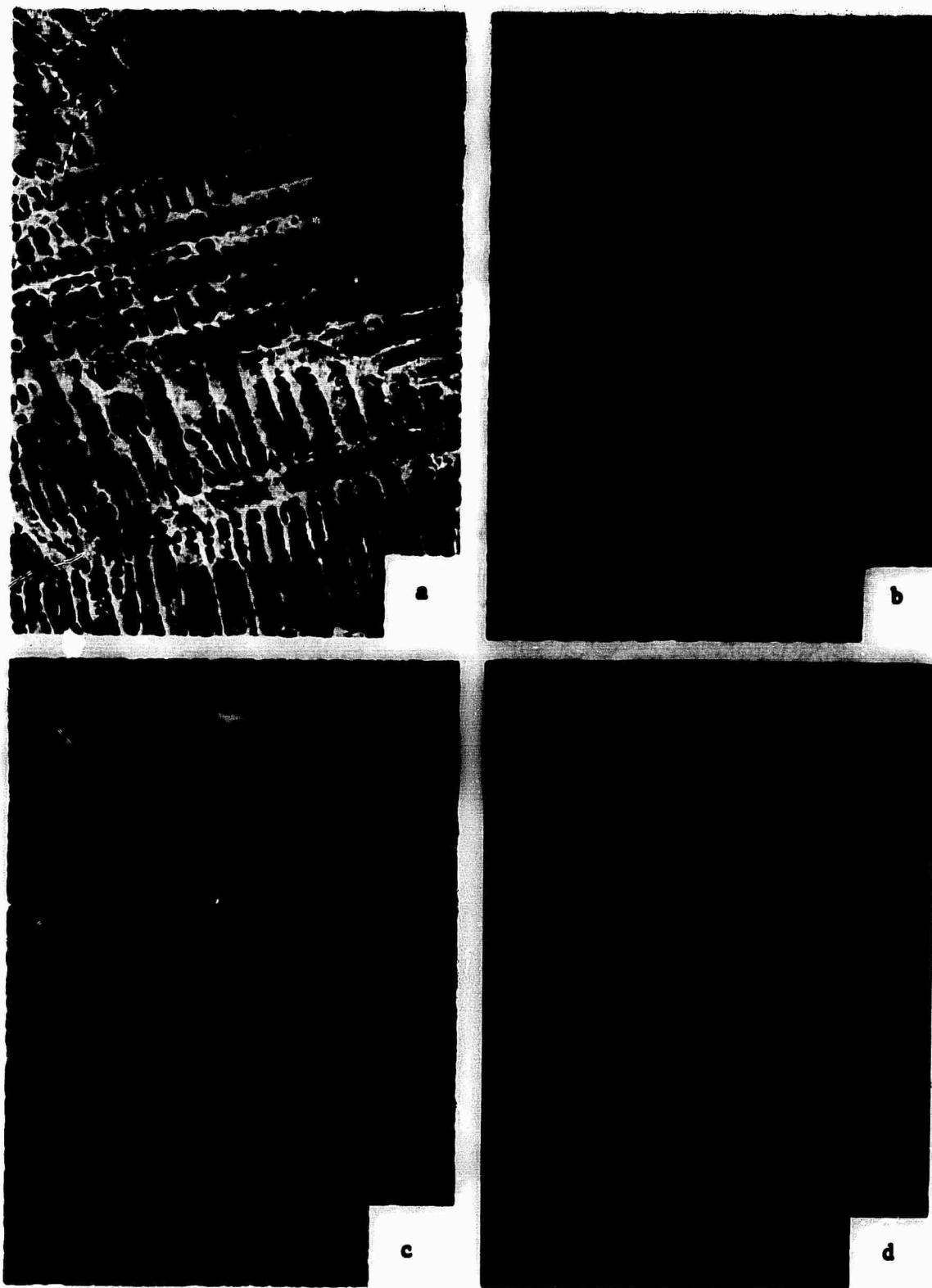


Figure 3. Variation of microstructure with cooling rate for maraging 300 alloy. (a) Gas quench, (b) liquid quench, (c) chill cast, (d) splat-cooled. Magnification 200X.

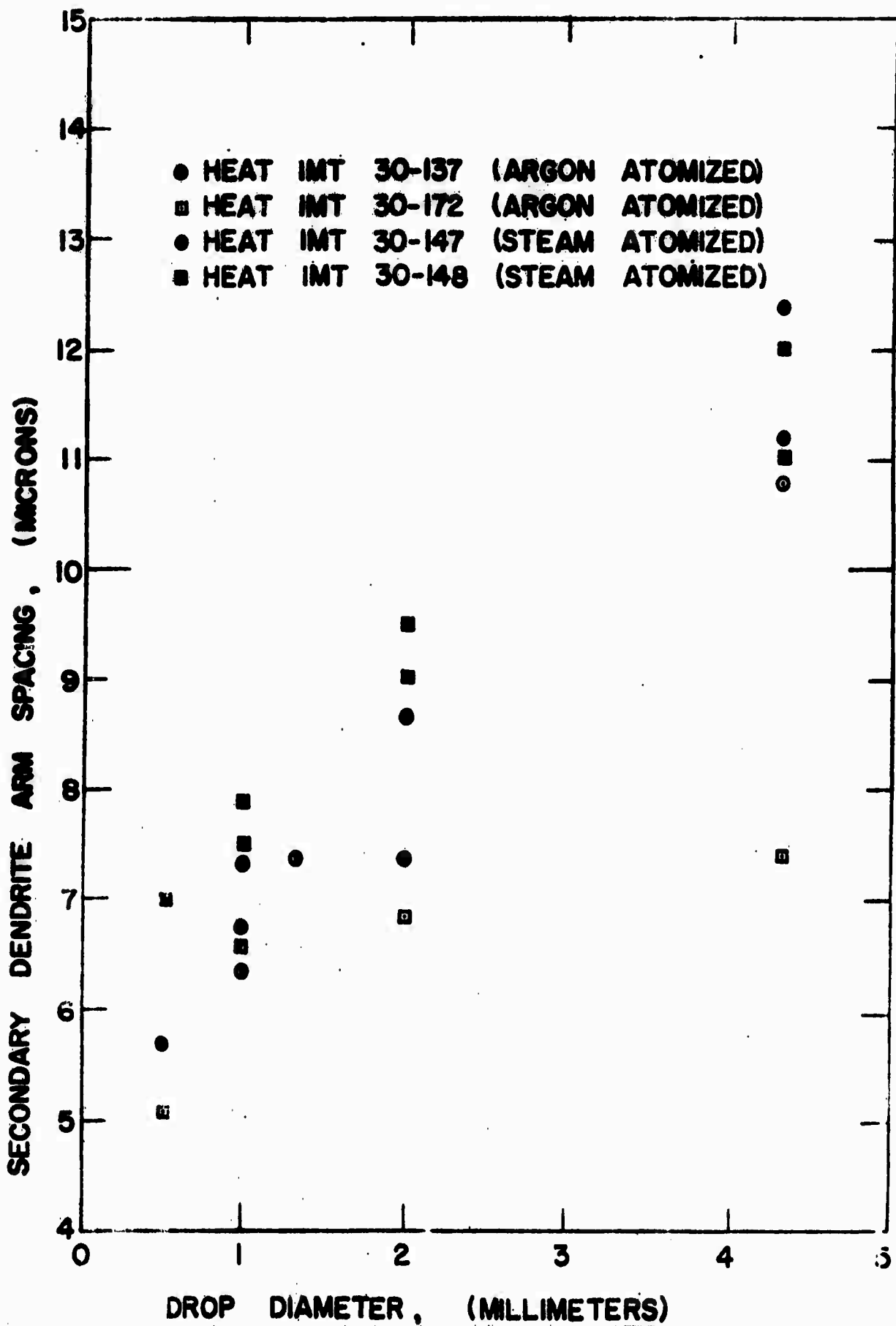


Figure 4. Secondary dendrite arm spacing versus diameter of coarse powders of atomized maraging 300 alloy.

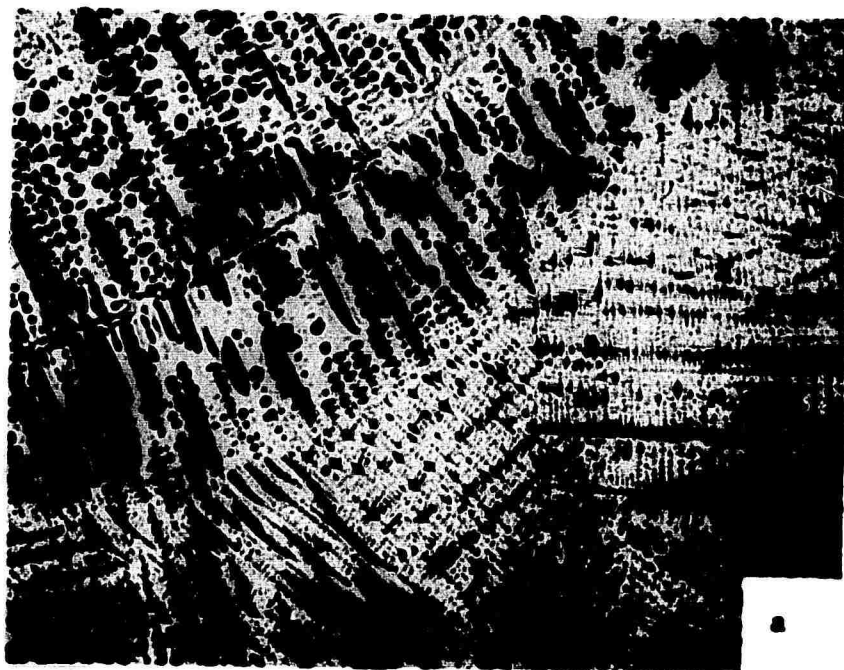


Figure 5. Duplex dendritic structure due to sudden variation in cooling rate. (a) Heat #30-148, mesh size -4/+5, (b) Heat #30-148, mesh size -8/+10. Magnification 75X.

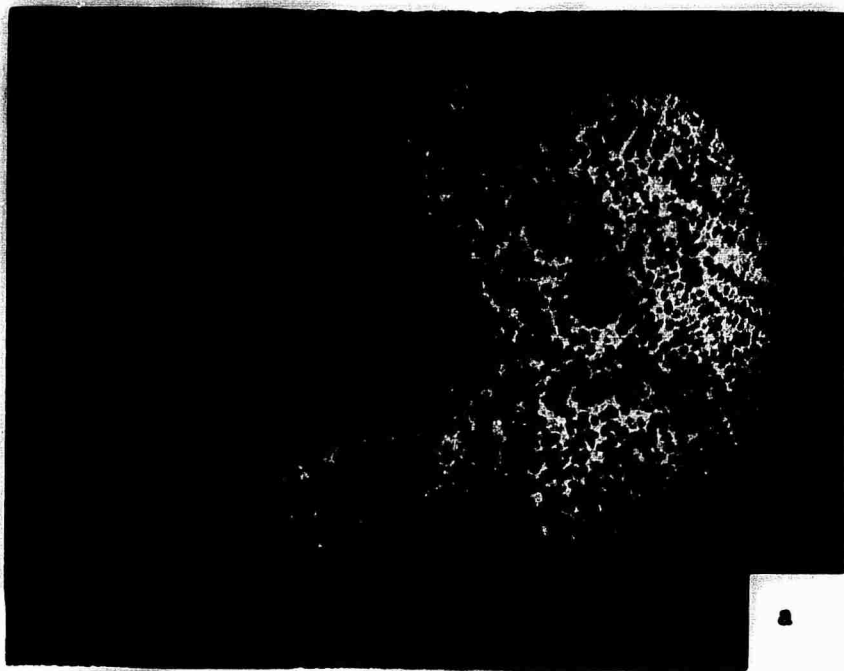


Figure 6. Photomicrographs of atomized coarse powder maraging 300 alloy, mesh size -16/+18. (a) Heat #30-148, steam atomized, (b) Heat #30-172, argon atomized. Magnification 100X.

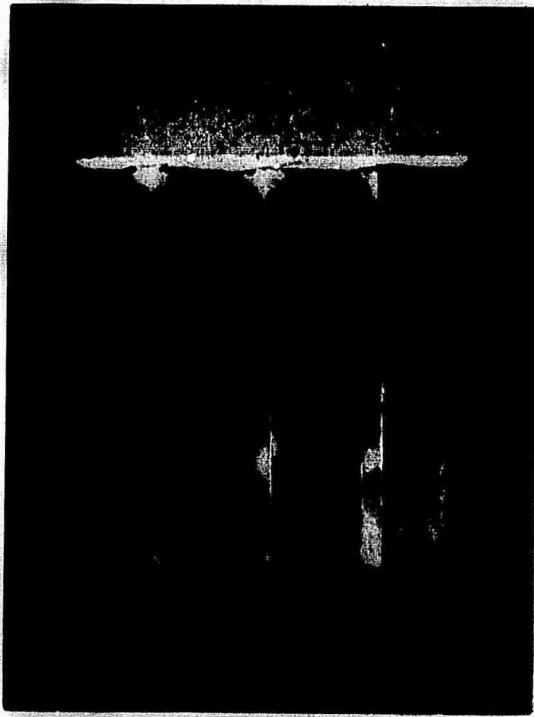


Figure 7. Photograph of the middle section of copper chill mold and cast rods of maraging 30C alloy. Top section is part of the pouring basin made from CO₂ sand.

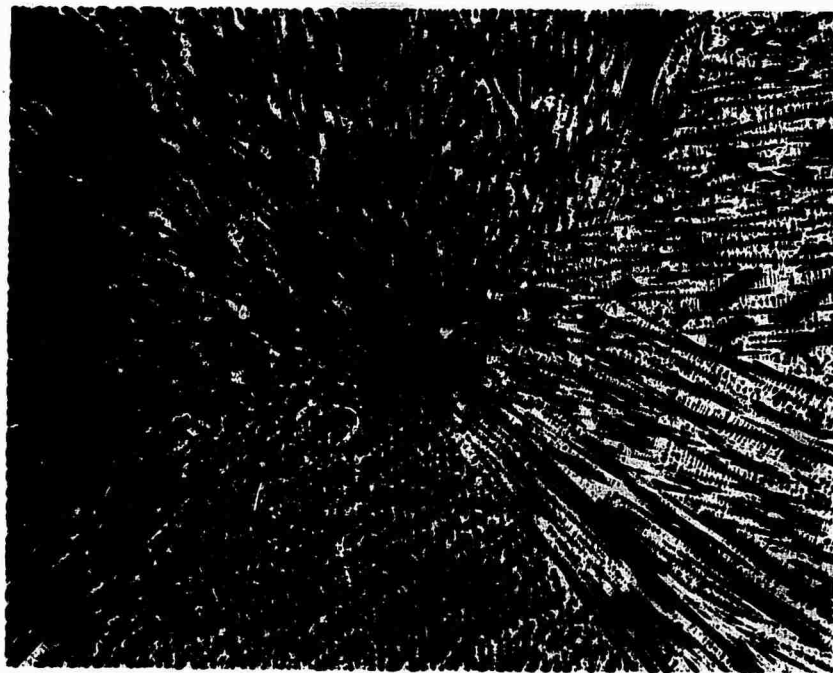


Figure 8. Photomicrograph showing the cross-sectional dendritic structure of rapidly solidified maraging 300 alloy rod. Magnification 50X.

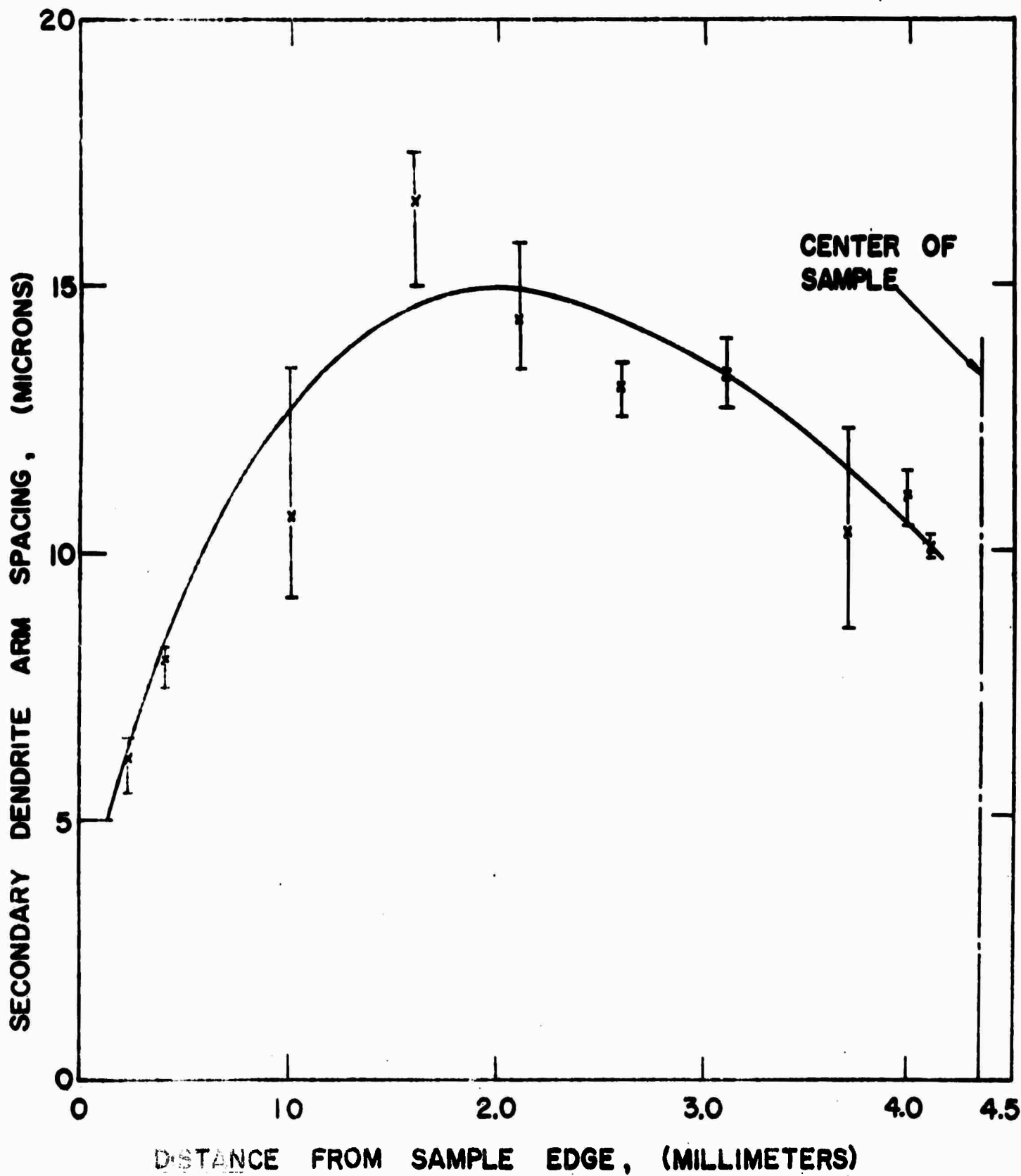


Figure 9. Secondary dendrite arm spacing versus distance from edge of 5/16" x 5/16" square rod of rapidly solidified maraging 300 alloy.

Task III and Task IV

THERMOMECHANICAL TREATMENTS

and

MICROSTRUCTURE AND MECHANICAL PROPERTIES

Heat Treatment and Aging of
300 Grade Maraging Steel

Material cut from a 1 3/4" diameter forged bar of Vascomax 300 was used to study the response of different aging times and temperatures upon the hardness. Banding (see section on metallography) in this barstock is more pronounced in the center of the bar than on the outside. Specimens cut from different sections (center and circumference) were therefore kept separate. The specimens were parallel ground on all sides so that hardness measurements in both longitudinal and transverse directions of the bar could be made. The specimen size was 3/16" x 1/4" x 3/4".

All specimens were solutionized in air at 1500°F for one hour. The average hardness after solution treatment is 31.6 R_C. Aging for 1, 3, 8 and 24 hours at 800, 850, 900 and 950°F was carried out in air in a furnace with a temperature control better than ±2°F. The specimens were polished on 600 paper to remove the thin oxide layer developed during aging.

Only minor and nonsystematic differences (0.5 R_C or less) in hardness for each aging treatment were found for longitudinal and transverse directions and for different sections of the bar. Table 1 gives the average of 12 hardness measurements for each aging temperature and time.

Table 1.

Hardness of maraging steel (Rockwell C) after different aging temperatures and times.

	<u>800°F</u>	<u>850°F</u>	<u>900°F</u>	<u>950°F</u>
<u>1 hr.</u>	—	48.9	50.2	51.1
<u>3 hrs.</u>	48.7	52.1	52.2	51.7
<u>8 hrs.</u>	51.8	53.3	53.0	51.9
<u>24 hrs.</u>	54.0	53.5	53.2	—

The recommended aging treatment for 300 grade maraging steel is 3 hours at 900°F. Our data show that a higher hardness can be obtained by aging at lower temperatures for longer times. This is a confirmation of earlier research⁽¹⁾. For practical applications a short aging time is of course desirable and a 3 hour aging treatment at 900°F gives a hardness close to the maximum obtainable.

Metallography

Banding is a recurring problem in maraging steels. The bands show up on polished sections after a one-half to two minute etch with 15% nital. Different explanations have been given for this problem^(2,3) but all agree that it is due to segregation of alloy constituents in the ingot.

A longitudinal cut through the center of the bar showed a moderate degree of banding as seen in photograph #1. The heaviest banding was observed near the center of the bar. Photograph #2 shows stringers of inclusions running parallel to the bands and to the direction of rolling.

The inclusions are Ti_2S (τ phase) and $Ti(C,N)$ as shown in photographs 3 and 4 respectively. These are the normal inclusions found in maraging steels⁽⁴⁾.

Tensile Properties

Tensile specimens were machined from different sections of the bar and tested after solutionizing and after aging. The specimens had a 0.160" diameter (1" long reduced section) and were tested on an Instron machine with a strain rate of 0.05"per minute. An extensometer was used in each case.

All the results are given below in table form. Included are some results from IMT material #3148 (atomized and extruded Vascomax 300).

Material taken from the center of the bar shows less ductility than material taken from the outside for both solutionized and for fully heat treated specimens. The values for UTS and 0.2% offset are in good agreement with values reported in the literature. The IMT material shows very much less ductility, especially in the aged condition. The UTS and 0.2% offset have only changed little. The material contains a large number of inclusions, some of which are over 100 microns in diameter. A microprobe analysis showed that the inclusions contain Ti and Al and some Fe, Ni, Co and Cr. It was concluded that the inclusions are oxide particles formed during atomization.

The scanning electron microscope was used to study the fracture surface of the tensile specimens. The surface of specimens in the solutionized and in the aged condition have the appearance of a fully ductile fracture surface. No cleavage or intergranular fracture was

Table 2.

Tensile properties of 300 grade Maraging steel.

	$\frac{A_0 - A_f}{A_0}$	$\frac{A_u - A_f}{A_0}$	$\epsilon_f = \ln \frac{A_0}{A_f}$	$\epsilon_f = \ln \frac{A_u}{A_f}$	UTS	0.2% offset	Young's Modulus	Work hardening rate
	per cent	per cent			ksi	ksi	ksi x 10 ⁻³	
Vascomax 300								
center	72.1	71.9	1.27	1.27	145.0	120.0	23.8	0.02
outside	76.0	75.8	1.43	1.42	145.8	138.8	22.5	0.02
Vascomax 300								
center	48.6	48.6	0.67	0.67	280.0	272.5	25.0	0.02
outside	53.6	53.2	0.76	0.76	274.0	269.0	28.0	0.02
aged 3hrs 900°F								
IMT	44.8	46.2	0.61	0.59	163.0	100.0	27.0	0.03
#3148	13.0	12.5	0.14	0.09	247.0	235.0	29.0	0.016

detected anywhere on the fracture surface. Photograph #5 shows the shear lip of specimen #8 (aged for 3 hours at 900°F). The void size is seen to be quite uniform except for some very large voids. The large voids contain inclusions. Picture #6 is a photograph of one of these areas at a higher magnification.

The fracture surface of the IMT material shows a large number of inclusions (picture #7) but is still fully ductile.

Fatigue

Fatigue specimens with a 0.15" diameter, 0.3" long reduced section, were machined from the same commercial bar and aged for 3 hours at 900°F in air. The specimens were tested in tension-compression on a Baldwin SF-1 fatigue testing machine. The results of all tests are given in Table 3. A plot of life vs load is shown in figure 8. Table 3 also shows the hardness of the specimens after aging and testing. No correlation between hardness and life at a particular load was found. Similarly, there does not seem to be much difference if the specimens are taken from the center or the circumference of the bar. At 90 ksi specimens 5, 6 and 12 are from the circumference; specimen 11 is from the center. At 80 ksi specimens 8, 10, and 13 are from the circumference and specimen 7 from the center. The scatter in the data is however not uncommon for these high strength materials.

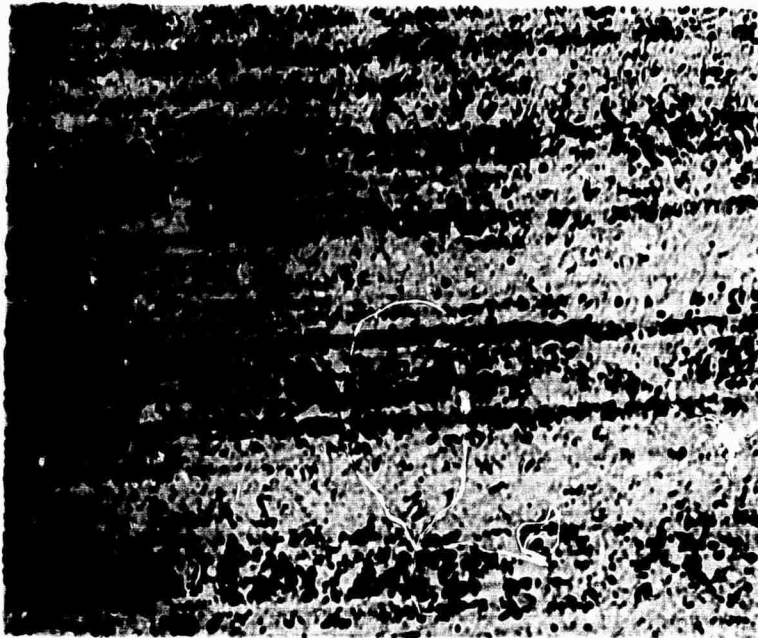
Table 3.

Fatigue data of Vascomax 300 in aged condition.

<u>Specimen</u>	<u>Load ksi</u>	<u>Life cycles x 10³</u>	<u>Hardness R_c</u>
1	200	15	53.0
2	150	20	52.7
3	120	41	52.3
4	100	80	52.3
5	90	72	52.5
6	90	274	53.2
11	90	218	53.0
12	90	2273	52.7
7	80	498	52.9
8	80	116	52.9
10	80	423	52.6
13	80	937	52.9
9	70	5330	specimen did not break

References

1. D. T. Peters and C. R. Cupp: The Kinetics of Aging Reactions in 18% Ni Maraging Steel. *Trans. Met. Soc. AIME*, 236 (Oct. 1966), pp. 1420-1429.
2. A. Goldberg: Morphology of Martensite Formation in a 300 Grade Maraging Steel. *Trans. ASM*, 62 (January 1969), pp. 219-229.
3. P. H. Salmon Cox, B. G. Reisdorf and G. E. Pellisier: The Origin and Significance of Banding in 18 Ni Maraging Steel. *Trans. Met. Soc. AIME*, 239 (November 1967), pp. 1809-1817.
4. T. Boniszewski and Elspeth Boniszewski: Inclusions in 18 Ni-Co-Mo Maraging Steel. *J. Iron and Steel Institute*, 204 (April 1966), pp. 360-365.



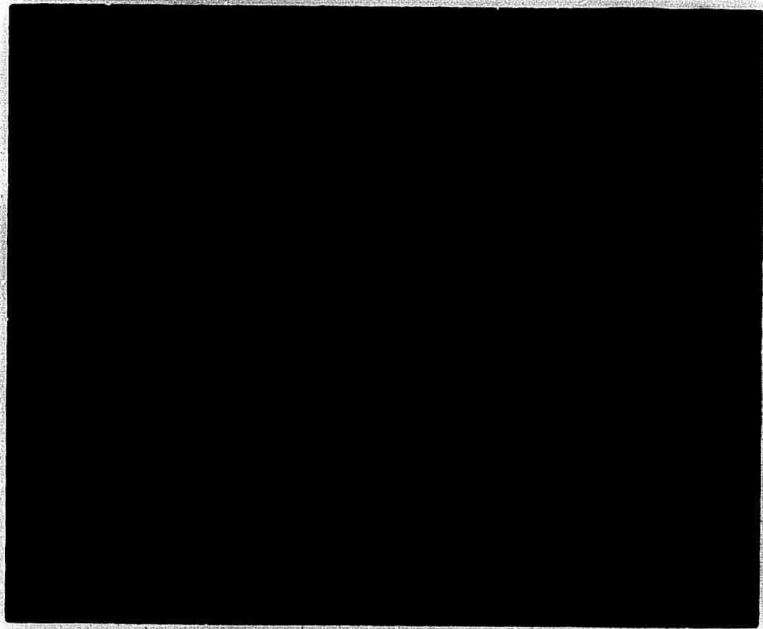
75X

Figure 1. Banding in commercial 300 grade Maraging Steel. 15% nital etch, 30 sec.



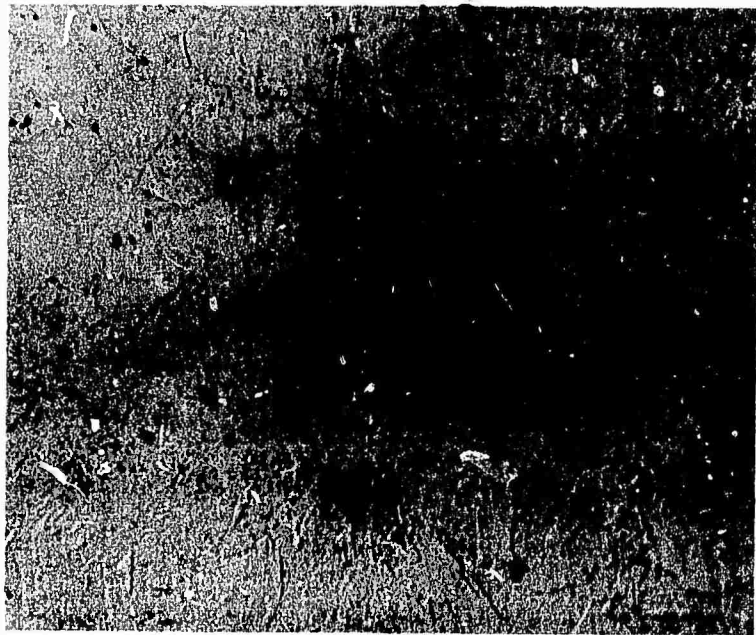
150X

Figure 2. Stringer of inclusions in commercial 300 grade Maraging Steel. 15% nital etch, 1 minute.



750X

Figure 3. Ti_2S (τ phase) inclusions in commercial 300 grade Maraging Steel.



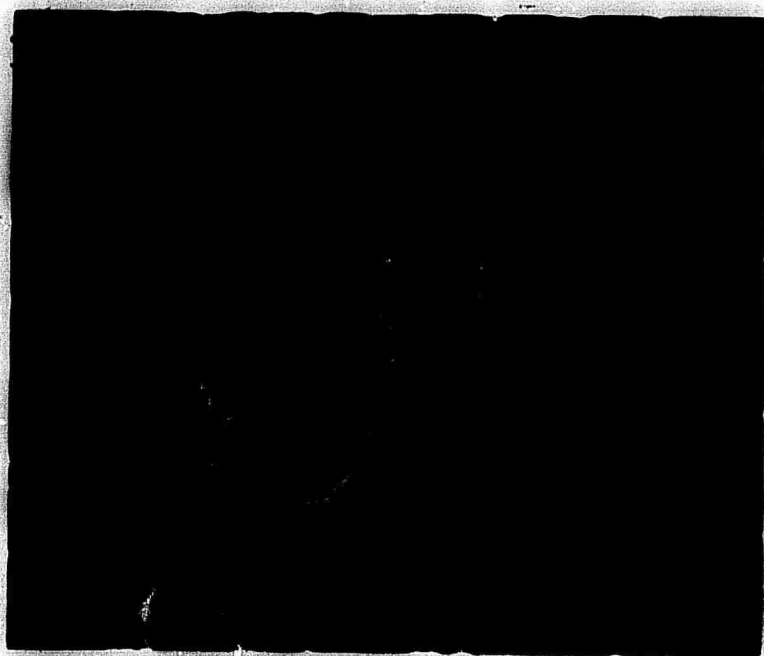
750X

Figure 4. $Ti(C,N)$ inclusions (square particles) in commercial 300 grade Maraging Steel.



550X

Figure 5. Fracture surface of aged 300 grade Maraging Steel. Note the inclusions in the large voids.



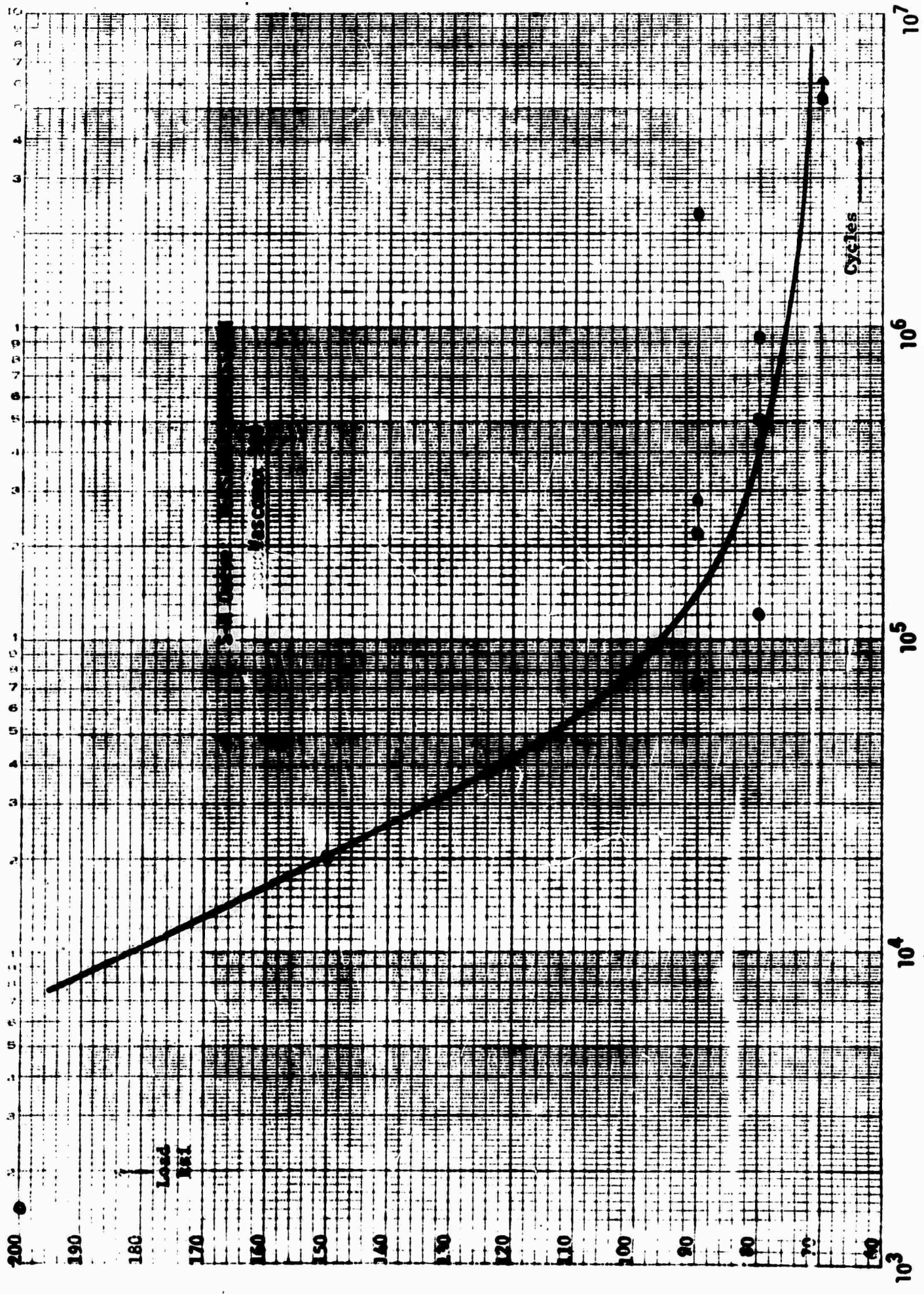
2200X

Figure 6. Large void on the fracture surface of aged Maraging Steel containing inclusions.

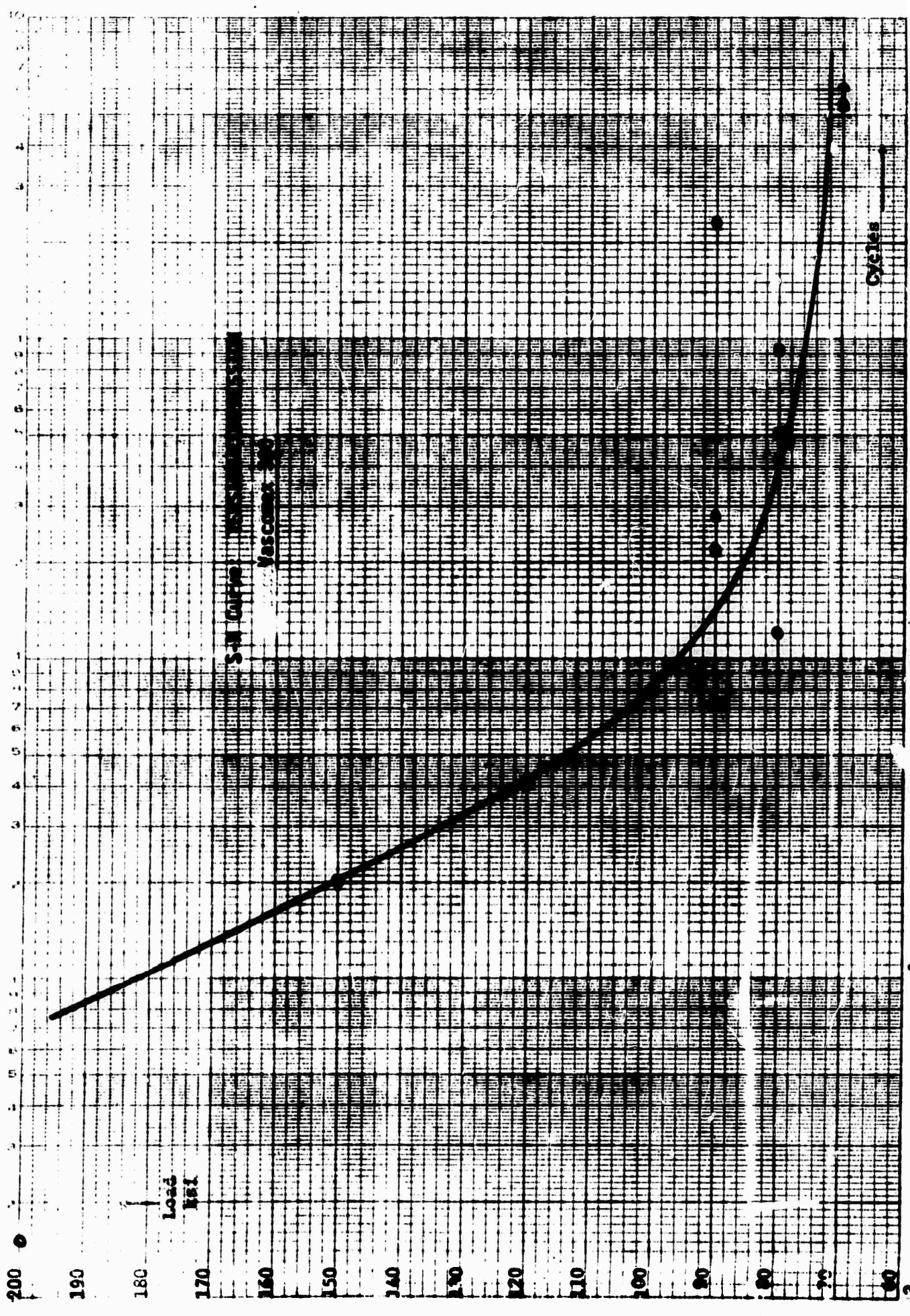


2690X

Figure 7. Fracture surface of atomized and extruded Maraging Steel. Note the large number of inclusions present in this material.



15 300 3000 JETZEN GRAPH PAPER
SER. 10487-105
4 CIRCLES PER DIV. 100 PLS. INCH



1

TASK IV - MICROSTRUCTURE AND MECHANICAL PROPERTIES
(Tensile Properties and Stress Corrosion Cracking)

Personnel

A.S. Argon, Professor of Mechanical Engineering
K. Ghosh, Visiting Engineer
R.A.S. Lee, Research Assistant

Research Report

Introduction

Although some initial planning on the program was done during the summer of 1970, the actual investigation commenced on September 15 with the addition of K. Ghosh and R.A.S. Lee to the program.

Work progressed in the following three areas: computations of strain fields and triaxial stresses in the neck region of a tensile specimen; tensile deformation experiments; design and manufacture of equipment for stress corrosion cracking experiments.

I Plastic Strain and Triaxial Stress Fields in the Neck of Circumferentially Grooved Tensile Specimens -(some of this work has been performed jointly under an NSF Sponsored Program on ductile fracture)

To determine the local conditions of triaxial stress necessary for hole formation by tearing away of the matrix from the inclusion, two limiting yield solutions were investigated. The triaxial stress state along the median plane of the neck, normal to the axis and along the specimen axis were calculated from a) the elasticity solution of Neuber for a Poisson's ratio of 1/2 to simulate a linearly hardening continuum, and, b) the generalized approximate solution of Bridgman for a non-hardening rigid material. The following analytical expressions were established:

- a) For a linearly hardening material with negligible yield stress, the triaxial stress at any point having coordinates $(r, \text{ and } z)$ [see FigIV-1]

$$\frac{\Sigma_T}{c} = \frac{\sqrt{(\zeta^2 + \rho^2 - 1)^2 + 4\zeta^2} - (\zeta^2 + \rho^2 - 1)}{(\zeta^2 + \rho^2 - 1)^2 + 4\zeta^2}$$

where $\zeta = \frac{z}{c}$, $\rho = \frac{r}{c}$; $c = \frac{a\sqrt{\frac{a}{R} + 1}}{\frac{a}{R}}$ and

$$c = \frac{1}{2\sqrt{2}} \frac{1 + \frac{a}{R} + \sqrt{\frac{a}{R} + 1}}{2 + \frac{a}{R} + \sqrt{\frac{a}{R} + 1}}$$

while $p = \frac{P}{\pi a^2}$ is the nominal stress across the neck.

b) For a non-hardening rigid material with yield stress Y .
The triaxial stress along the median plane ($z = 0$).

$$\frac{\Sigma_T}{Y} = \left[\ln \left(\frac{2aR + a^2 - r^2}{2aR} \right) + 1/3 \right]$$

The triaxial stress along the axis ($r=0$) for $z < a\sqrt{1 + \frac{a}{2R}}$

$$\frac{\Sigma_T}{Y} = \left[4 + \ln \left(\frac{2aR + a^2}{2aR} \right) \right] \exp \left(- \frac{z^2}{4(a^2 + 2aR)} \right) - \frac{11}{3}$$

As is clear from inspection of the equation above, in a linearly hardening material with quasi-elastic loading behavior the maximum triaxial stress occurs on the surface of the necked region while in the non-hardening material it is in the center of the necked region. For this reason fracture initiation should occur on the surface in a rapidly hardening material and in the interior in a non-hardening material.

To determine the local equivalent plastic strain necessary for hole formation by tearing away of the matrix from the inclusion a geometrical calculation was performed based on the Bridgman model leading to the following solution for a point on the specimen axis.

$$E^{-P} = \ln \left(\frac{R_0'^2 (1 - \cos \alpha_0)}{R_1'^2 (1 - \cos \alpha_1)} \right)$$

Where the quantities R_0' , R_1' , α_0 and α_1 , defined in Fig. IV-1 are calculable by a computer program from the initial and final geometries of the neck region of the specimen.

Based on the above analysis it will be possible: a) to give bounds for the triaxial stress and total plastic strain for inclusion separation, by measuring the coordinates of the inclusion which is seen in the axial - micro section to have separated from the matrix; and b) to determine the same parameters of triaxial stress and plastic strain for actual fracture by hole growth.

II Tensile Deformation of Vascomax 300

Tensile experiments were performed on Vascomax 300 maraging steel in both the as received condition and the austenitized-quenched-and-aged condition. The results of these experiments are as follows:

a) As Received Vascomax 300

Both smooth bar and pre-grooved round tensile specimens were strained to fracture at room temperature. The true stress-strain curve of the smooth bar for this material is shown in Fig. IV-2. As can be seen, the material yields gradually over a strain range of 0.03 and reaches flow stress of 150 ksi which rises slowly and nearly linearly to 175 ksi at a strain of 0.62 where fracture occurs. In the flow region the strain hardening rate is 42 ksi. These results are summarized in Table IV-1.

The dependence of the true strain to fracture on the triaxial tensile stress was investigated by a series of circumferentially grooved tensile specimens of different initial neck radii of curvature. The results of these experiments are summarized in Table IV-2, and in Fig. IV-3.

b) Austenitized-quenched and aged (at 900° F) Vascomax 300

The same experiments outlined in part a) were performed on hardened Vascomax 300 specimens. The stress-strain curve of the material is shown in Fig. IV-2. Yielding again occurs gradually and is complete after a strain of 0.03, where a flow stress of 230ksi is reached. The strain to fracture is now markedly reduced and occurs at a strain of 0.11.

The dependence of the true strain to fracture on triaxial tensile stress obtained by circumferentially grooved specimens is shown in Fig. IV-3, and also summarized in Table IV-2.

Evidently the effect of aging is to reduce the strain to fracture drastically. How this comes about by a change of precipitate size and spacing is now under investigation. Also under investigation are the conditions of hole nucleation by inclusion tear-away.

Furthermore, a bar of hot, isostatically pressed Vascomax 300 has been obtained from IMT for a parallel comparative investigation.

III Plane-Strain Fracture Toughness and Stress Corrosion Cracking Experiments

A considerable amount of time was expended in surveying the literature and gathering up-to-date information on plane strain fracture toughness testing via the so-called "Manjoine" specimen and the constant stress intensity specimen of wedge geometry.

Two simple scissor shaped test frames made of Hastaloy are now under construction for stress corrosion cracking experiments in chloride solutions. The test frames, loaded by compression springs and equipped with load cells and LVDT extensions will be capable of measuring crack growth rates in constant-stress intensity, wedge shaped specimens. These experiments on both commercial Vascomax 300 and hot-isostatically pressed Vascomax 300 will commence within February.

TABLE IV - 1

Tensile Behavior of Vascomax 300

	Yield Stress ksi	Strain-Hard Rate ksi	U.T.S. ksi	Uniform Strain	Reduction of Area
Unaged	150	42	220	0.027	0.710
Aged	230	45	262	0.06	0.512

TABLE IV - 2

Tensile Ductility under Triaxial Stress of Vascomax 300

Unaged Vascomax 300
(all dimensions in inches)

R_0	a_0	R	a	a/R	Red. Area	σ_T/Y	E_f
0.125	0.125	0.068	0.145	2.13	0.665	1.058	1.09
0.250	0.125	0.098	0.141	1.44	0.682	0.876	1.15
0.500	0.125	0.112	0.138	1.23	0.696	0.816	1.19
1.250	0.125	0.182	0.129	0.71	0.733	0.666	1.32
∞	0.125	0.082	0.067	0.67	0.710	0.710	1.23

Aged Vascomax
(all dimensions in inches)

R_0	a_0	R	a	a/R	Red. Area	σ_T/Y	E_f
0.125	0.125	0.101	0.220	2.18	0.226	1.070	0.256
0.250	0.125	0.112	0.208	1.86	0.307	0.991	0.368
0.500	0.125	0.134	0.189	1.41	0.430	0.868	0.559
1.250	0.125	0.164	0.176	1.07	0.505	0.758	0.702
∞	0.125	0.208	0.087	0.42	0.512	0.524	0.714

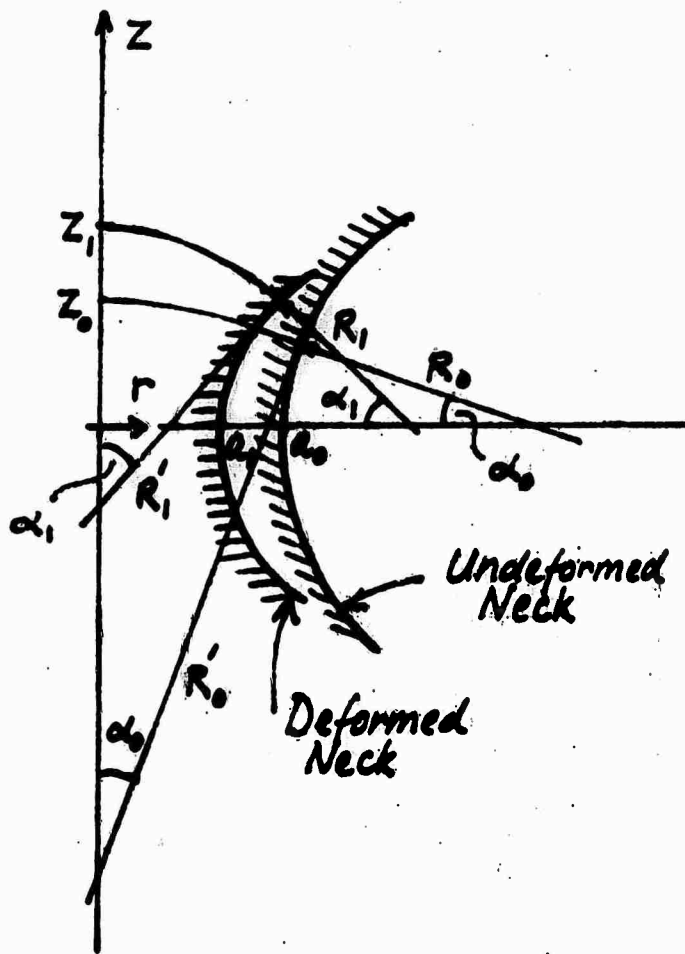


Fig. IV-1 Geometry of the undeformed and deformed neck in circumferentially grooved specimens.

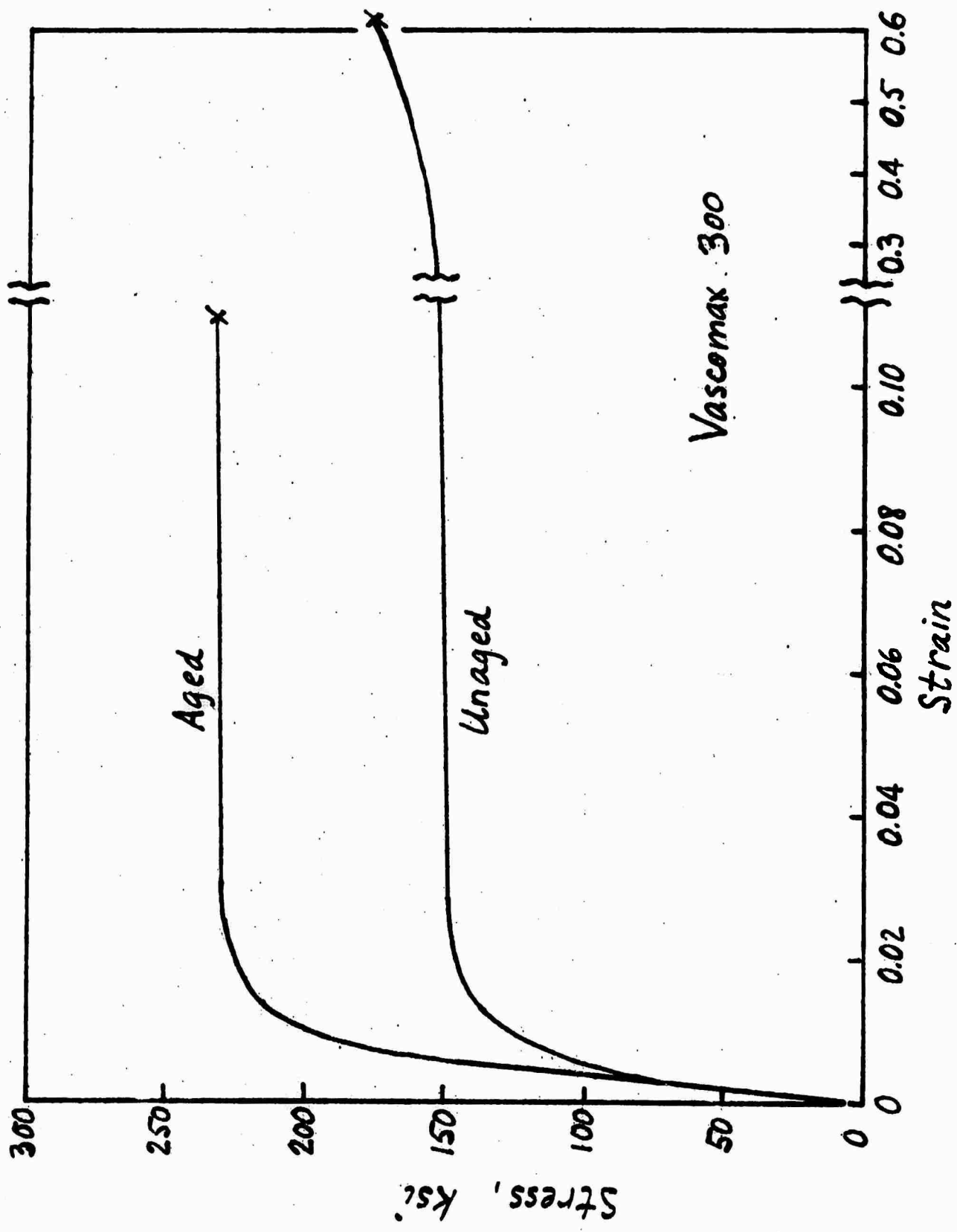


Fig. IV - 2 Stress - strain curves at room temperature of Vascomax 300

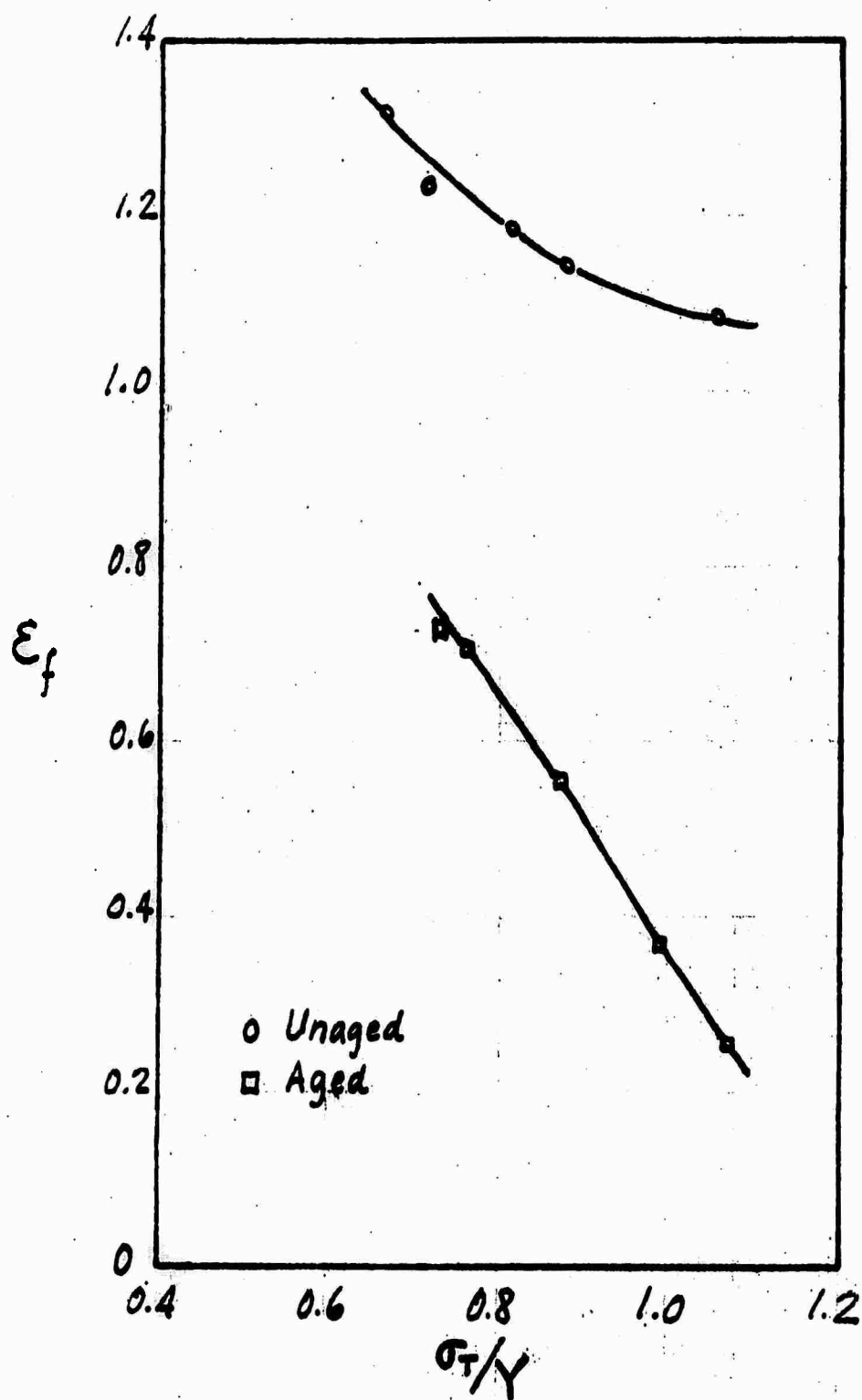


Fig IV -3 Dependence of strain to fracture on triaxial tensile stress in Vascomax 300